Metasomatism induced by alkaline magma in the upper mantle of northern Victoria Land (Antarctica): an experimental approach

Cristina Perinelli[1], Andrea Orlando[2], Aida Maria Conte[3], Pietro Armienti[1], Daniele Borrini[4], Barbara Faccini[5] & Valeria Misiti[6]

[1]*Dipartimento di Scienze della Terra, Università di Pisa, via S. Maria 53, 56100 Pisa, Italy*

(cperinelli@dst.unipi.it)

[2]*C.N.R.-I.G.G. U.O. di Firenze,via G. La Pira, 4 - 50121 Firenze, Italy*

[3]*C.N.R.-I.G.G. U.O. di Roma, p.le Aldo Moro 5, 00185 Roma, Italy*

[4]*Dipartimento di Scienze della Terra, Università di Firenze,via G. La Pira, 4- 50121 Firenze, Italy*

[5]*Dipartimento di Scienze della Terra, Università di Ferrara, via Saragat 1, 44100, Ferrara, Italy*

[6]*I.N.G.V. Sezione di Sismologia e Tettonofisica, via di Vigna Murata 605, 00143, Roma, Italy*

Corresponding author: Cristina Perinelli

ABSTRACT

Magma generation in the Ross Sea system is related to partial melting of strongly metasomatised mantle sources where amphibole most probably plays a crucial role. In this context, metasomatism induced by a mela-nephelinite melt in lithospheric mantle of the Mt. Melbourne Volcanic Province (northern Victoria Land – NVL, Antarctica) was investigated experimentally studying the effects of melt interaction with lherzolite at 1.5-2.0 GPa and T=975-1300°C, and wehrlite at 1.0 GPa and T=1050-1250°C. The experiments were designed to induce melt infiltration into the ultramafic rocks. The observed modifications in minerals are compared with those found in mantle xenoliths from NVL. The effects of metasomatic modifications are evaluated on the basis of run temperature, distance from the infiltrating melt and on the diffusion rates of chemical components. Both in lherzolite and wehrlite, clinopyroxene exhibits large compositional variations ranging from primary diopside to high Mg-Cr-(Na) augitic and omphacitic clinopyroxenes in lherzolite, and to low Mg and high Ti-Al-Fe-Na augites in wehrlite. Olivine (in wehrlite) and spinel (in lherzolite) also result compositionally modified, the former shows enrichments in Fe, the latter displays a higher Cr/(Cr+Al) ratio. The systematic variations in mineral compositions imply modifications of the chemistry of the infiltrating melt as recorded by the glass veinlets and patches observed in some charges. In experiments involving wehrlite paragenesis, the glass composition approaches that of melt patches associated to both amphibole-free and amphibole-bearing natural samples, and is related to olivine+clinopyroxene crystallisation coupled with primary clinopyroxene dissolution at the contact between the metasomatising melt and the solid matrix. Even if amphibole crystallisation was not attained in the experiments, we were able to explain the occurrence of amphibole in the natural system considering that in this case a hot metasomatising melt infiltrates a cooler matrix.

Key words: Mantle metasomatism, lherzolite, wehrlite, melt-rock reaction experiments, Antarctica

INTRODUCTION

The Ross rift system and accompanying Cenozoic volcanism of the Mt. Melbourne Volcanic Province (northern Victoria Land, Antarctica) has been related either to the occurrence of a long lasting mantle plume or to the top-down control of the tensile state of the lithosphere (Rocholl *et al.*, 1995; Rocchi *et al.*, 2006). Alkali-basaltic eruptions brought to the surface abundant mantle xenoliths, mainly represented by both amphibole-free and amphibole-bearing spinel peridotites and cumulitic pyroxenites-wehrlites which can provide information on the thermal state and on chemical and mineralogical composition of lithospheric mantle.

Previous studies have revealed a significant mineralogical and compositional heterogeneity of NVL upper mantle, due to the combined effects of partial melting and both modal and cryptic metasomatic processes (Coltorti *et al.*, 2004, 2006; Perinelli *et al.*, 2006). Modal metasomatism of NVL mantle xenoliths is recognizable by the occurrence of pargasitic to kaersutitic amphibole, usually associated with glass. Amphibole may forms veins or grows as disseminated grains around clinopyroxene and/or spinel. Disseminated and vein amphiboles have similar major and trace element composition and their genesis is attributed to the reaction of lherzolitic rocks with an infiltrating magma, possibly an undersaturated, TiO_2-rich Na alkaline silicate melt (Coltorti *et al.*, 2004). According to these authors, the reaction that generates amphibole first produces progressive modifications on primary mantle paragenesis forming secondary olivine (ol2-nat), clinopyroxene (cpx-A) and spinel (sp2-nat) besides consuming orthopyroxene. These neo-formed phases represent "precursors" of amphibole as well being associated with it. Coltorti *et al.* (2004) inferred that the possible metasomatic agent was similar to the most undersaturated rock found in the Province, a nephelinite outcropping at Greene Point (sample SAX20, Orlando *et al.*, 1997; Perinelli *et al.*, 2006). An analogous nephelinitic melt has been considered to be responsible for the metasomatic events recognized in wehrlites and pyroxenites outcropping in the same area by Perinelli & Armienti (2005).

The concurrent presence of amphibole-free and amphibole-bearing spinel peridotites and pyroxenites has been documented in different areas worldwide (Xu & Bodinier, 2004 and references therein). They may result from the same metasomatic event (Xu & Bodinier, 2004) but are related to two different mechanisms: *i*) "wall-rock" metasomatism, due to the transport of melt in fractures (veins and dykes), and *ii*) "diffuse" metasomatism related to percolation of small melt fractions along grain boundaries in a solid matrix. The differences

on metasomatic assemblage and mineral compositions (major and trace elements) in the xenoliths can be explained by the P-T control on amphibole stability and the progressive chemical variation of infiltrating melts (Xu & Bodinier, 2004).

Despite the interest in completely highlighting how "diffuse" and/or "wall-rock" metasomatism acts, few experimental studies on interaction of alkaline melts with mantle rocks have been undertaken (e.g. Sean & Dunn, 1994; Shaw *et al.*, 1998; Rapp *et al.*, 1999; Shaw, 1999). Therefore, in order to better understand the processes involved in the metasomatism in NVL mantle, a series of high pressure – high temperature experiments were performed to simulate *in situ* the effect of different extent of metasomatism. In particular, the aim of experiments was i) to investigate the reactions affecting lherzolite/wehrlite phases during interaction with alkaline melts and ii) to test the possibility that ensuing reactions generate amphibole.

Experiments were performed at pressure conditions of 1.5-2.0 GPa for lherzolite and 1.0 GPa for wehrlite in a P - T range close to the conditions of metasomatism that may have occurred in nature, according to Perinelli *et al.* (2006).

STARTING MATERIALS

Nephelinite-lherzolite runs at high T (>1100°C): fine grained (<100 μm) nephelinite SAX20 (sampled at Green Point) containing olivine phenocrysts (Fo_{71-78}) (Table 1) scattered in a groundmass consisting of diopsidic clinopyroxene, feldspar ($Ab_{49}Or_{47}An_4$), nepheline ($Ne_{66-70}Ks_{3-6}Qtz_{23-30}$) and spinel (magnetite$_6$-ulvospinel$_{94}$ series).

Anhydrous lherzolite (<50 μm) from a xenolith (sample 154L, provided by M. Coltorti) was chosen as representative of unmetasomatised mantle. Mineral compositions are given in Table 1.

Nephelinite-lherzolite runs at low T (<1100°C): In these runs we used the 154L lherzolite and a *SAX20 glass_5bru* glass obtained melting in air SAX20 powder at T=1400°C (quenched after 2 minutes) in a Deltech DT-31VT-OS2 vertical quench furnace and re-melting the resulting glass at the same T, after grinding. A 5 wt.% of 99.9% pure natural brucite ($Mg(OH)_2$) powder was added to the (anhydrous) glass since its decomposition at

run conditions (Irving et al., 1977) supplies water to the system (Table 1). Moreover, another glass (*SAX20-2.5TiO$_2$glass_5bru*) was prepared adding 2.5 wt.% TiO_2 to SAX20 prior to the 2 melting cycles at 1400°C; as in the preparation of the previous starting material, 5 wt.% of 99.9% pure brucite was added to the mixture before loading the capsule.

MgO and TiO_2 additions allow the bulk composition of the glass to approach that of metasomatic melts inferred by Coltorti *et al.* (2004) (Table 1) and water released by brucite enhances reaction rates and counterbalances the water loss during glass synthesis.

Nephelinite-wehrlite runs: Nephelinite SAX20 was used with a fresh wehrlite (BRP19), free of any metasomatic feature, sampled at Browning Pass, on the coast of Ross Sea, NVL. This rock is formed by ~ 50% olivine (Fo_{81}), ~ 50% diopsidic clinopyroxene and trace of Cr-spinel (Table 1).

EXPERIMENTAL AND ANALYTICAL PROCEDURES

Nephelinite-lherzolite runs

At T>1100°C nephelinite powder was placed at the bottom of a graphite capsule, to avoid Fe loss, and in close contact with lherzolite powder; the nephelinite/lherzolite ratio was ~ 1 in all runs. The graphite capsule (4 mm long) was then inserted into an outer Pt capsule (O.D.= 3.0 mm, I.D.= 2.8 mm, length ~ 7–8 mm) welded closed. Experiments were performed at 1.5 and 2.0 GPa, at temperatures in the range 1150-1300°C; runs lasted up to 95 hours. No H_2O was added to the charges.

$Ag_{50}Pd_{50}$ capsules were used in runs at T<1100°C. The melt-peridotite couples were assembled as sandwiches of lherzolite between either *SAX20glass_5bru* or *SAX20-2.5TiO$_2$glass_5bru* powders, again with a melt/lherzolite ratio of ~ 1. Due to the lower temperatures of these experiments, longer durations (190-212 hours) were used.

All of these experiments (Table 2) were done in a 1/2 inch piston-cylinder apparatus (at C.N.R.-IGG HP-HT lab, Florence) using a salt-Pyrex-crushable alumina assembly and the "hot piston-out" technique. Pressure was calibrated using the reaction ferrosilite = fayalite + quartz at T=1000°C (Bohlen *et al.*, 1980). Further experimental details are found in

Orlando & Borrini (2001). Temperature was measured by a Pt_{100}-$Pt_{90}Rh_{10}$ thermocouple and no correction for the effect of pressure was applied to the thermocouple e.m.f. Pressure was considered accurate ±0.05 GPa and temperature to ±5°C of stated values.

Oxygen fugacity during the experiments at T>1100°C was estimated according to the calculated Fe^{3+} in spinel coexisting with olivine and orthopyroxene (Ballhaus *et al.*, 1990) and the C-COH buffer (Ulmer & Luth, 1991). The two independent estimates are consistent, and give values of ΔFMQ<-1.2.

Run products were analyzed on a JEOL JXA-8600 electron microprobe operated at 15 kV accelerating voltage and 10 nA beam current. Count times ranged from 10 to 40 s (same times for backgrounds) and alkali loss was minimised by defocusing the electron beam up to 15 μm. Data were corrected for the matrix effect using the Bence & Albee (1968) method and errors were estimated according to Vaggelli *et al.* (1999).

Nephelinite-wehrlite runs

These samples were prepared by packing a layer of wehrlite powder over a layer of nephelinite powder in a graphite capsule, to obtain a wehrlite/nephelinite ratio of ~ 1 in all charges. The graphite capsule was put into a Pt capsule, stored in an oven at 110°C overnight to remove humidity, and then welded. The final length of capsules was 8-9mm.

All nephelinite-wehrlite experiments were run in a ¾ inch piston cylinder apparatus, at the HP-HT Laboratory of Experimental Volcanology and Geophysics of Istituto Nazionale di Geofisica e Vulcanologia (INGV), Rome.

Experiments were performed at 1.0 GPa at 1250 to 1050°C; run times were in the range 5-48 hours (Table 2). Experiments performed at 1150°C and 1050°C were repeated with ~3% water in the capsules. Later on we identify as "hydrous" the experiments with H_2O added in the charge and "anhydrous" the runs without H_2O addition, even if in this last experiments, water is present because of its occurrence in nephelinite (Table 1).

The pressure cell consists of a NaCl, Pyrex, graphite heater and magnesia inner sleeves assembly. The dimension of this assembly allowed running volatile-free and volatile-added charges at the same time. Al_2O_3 (anhydrous runs) or pyrophillite (water-bearing runs) powder was packed around the capsules (Freda *et al.*, 2001). The temperature was controlled by a $W_{95}Re_5$-$W_{74}Re_{26}$ (type C) thermocouple. The thermocouple tip was placed in the middle of ~10mm long hot spot between the two capsules (for further details see

Misiti *et al.*, 2006). The thermocouple was encapsulated in an Al_2O_3 sleeve. The temperature was considered accurate ±3°C of stated values.

Pressure was calibrated against the NaCl melting point (Bohlen *et al.*, 1980) at 1004°C at 1.0GPa and 1090°C at 1.5GPa. Pressure correction was +250bar.

Experiments were first pressurized up to the target pressure and then heated at a rate of 200°C/min up to 20 °C below the target temperature. A smaller rate of 40 °C/min was applied within the last 20 °C of heating to avoid overshooting. The experiment was ended by switching off the heating power while maintaining pressure constant. The initial quench rate was about 2000 °C/min. The pressure is considered accurate to ±0.05GPa and possible pressure effects on the e.m.f. of the thermocouple were ignored.

Oxygen fugacity estimated according to Ulmer & Luth (1991) is for all experiments ΔFMQ<-1.3. Experimental conditions and results are summarized in Table 2.

BSE images of nephelinite-wehrlite runs were collected at the Dipartimento di Scienze della Terra of Pisa University, using a Philips XL30 SEM.

Microanalyses of phase composition were performed on polished carbon-coated mounts by a 4-spectrometer Cameca SX50-52 electron microprobe using a 15-keV accelerating voltage, a 15 nA beam current (at C.N.R.-IGAG, Rome). Matrix effect corrections (ZAF) were performed using the algorithm of Philibert (1963) and Duncumb & Reed (1968). A focused beam was used for minerals, while glasses were analysed with the 10μm diameter beam to minimise volatilisation of sodium; a 5μm diameter beam was used for small volumes of glass in the lowest-temperature experiments.

RESULTS

Nephelinite-lherzolite runs

Phases detected in experimental products are reported in Table 2 and chemical analyses of lherzolite are shown in Table 3. In experimental runs glass is seldom found in lherzolite and is not related with the distance from the lherzolite/nephelinite interface as well as the occurrence and the composition of neo-formed phases (see below).

Runs at high T (>1100°C). Nephelinite was completely molten at P= 1.5 GPa, T= 1300°C. At lower temperatures it was partially molten and clinopyroxene + olivine, spinel

and nepheline progressively saturated the liquid with decreasing T. In the run at 2.0 GPa glass coexisted with clinopyroxene, olivine, spinel and rhönite (Table 2).

The lherzolite area of the charges contains small, rare glass pockets (mostly not-analysable by electron microprobe) with the exception of the run performed at the lowest T (Fig. 1a).

In the lherzolitic portion of the capsules at 1250°C, some glass analyses attain a SiO_2 rich latitic composition; The original phases, olivine (ol1), clinopyroxene (cpx1), orthopyroxene (opx1), spinel (sp1) are accompanied by scattered neo-formed subhedral clinopyroxene (cpx2, Fig. 1a) and spinel (sp2. Analyses of neo-formed phases in lherzolitic portion of the charges are reported in Table 3.

At 1.5 GPa, cpx2 is augite in all the runs: with respect to the original phases MgO increases (from 16.5-17.4 up to 26 wt.%), Na_2O (from 0.4-0.8 up to 2.2 wt.%) and Cr_2O_3 (from 0.4-0.9 up to 2.7 wt.%) also increase while CaO decreases (from 22.6-23.8 to 7.6 wt.%). In particular, in the run carried out at 1150°C neo-formed clinopyroxene is mainly found around orthopyroxene crystals together with not-analysable glass (Fig. 1b).

At 2.0 GPa cpx2 have greater Na_2O content (2.3-4.1 wt.%) than cpx2 synthesised at 1.5 GPa; their CaO content is generally low (9.7-14.2 wt.%) and Cr_2O_3 and MgO content ranges from 1.2 to 1.8 and from 17.4 to 18.4 wt.%, respectively. According to Morimoto (1989) classification, most of the analysed crystals are omphacite. Neo-formed spinel (sp2) occurs as subhedral crystals or coronas around original crystals in all the runs, as shown in Figure 1c. Sp2 crystals generally show higher Cr# (Cr/(Cr+Al); up to 0.85) and lower Mg# (Mg# = Mg/(Mg+Fe^{2+}); down to 0.63) with respect to sp1 crystals. The highest Cr_2O_3 content (67.2 wt.%) was found in experiment at 1150°C.

Runs at low T (<1100°C). Backscattered electron images reveal that some olivine crystals close to the lower interface sank into the nephelinitic portion and reacted from Fo_{90} to Fo_{85}. In these runs interaction occurred despite the low T, probably due to reactivity of glass as starting material and the long durations utilised (190-212 hours).

Run with ***SAX20glass_5bru***. In the nephelinitic portions of the capsule, glass is dominant and olivine (Fo_{78}), augitic clinopyroxene, rhönite and apatite crystals are commonly found. In the lherzolite, neo-formed phases join the original ones: olivine crystals equilibrated to Fo_{86} close to the lower interface (ol2) and small (<20 μm) enstatitic orthopyroxene crystals (opx2) enriched in Na_2O (0.5-1.4 wt.%) and CaO (1.1-1.6 wt.%) relative to opx1 are

sometimes found scattered in sporadic glass patches along the capsule walls. Glass analyses show very low totals (<70 wt.%) probably due to the combined effect of water content and of poorly polished surfaces of micro vesicular or friable glass (e.g. see Peterson & Newton, 1990). Neo-formed augite and omphacite, enriched in Na_2O (up to 3.3 wt.%) and Cr_2O_3 (up to 2.5 wt.%) and depleted in CaO (16.2-19.8 wt.%) with respect to cpx1, are found in the whole lherzolitic portion together with high Cr# (0.39-0.54) - low Mg# (0.59-0.60) neo-formed spinel.

Runs with ***SAX20-2.5TiO$_2$glass_5bru*** (Ti-doped). At 1025°C, glass is the dominant phase in the nephelinitic portions of the charge, however small (<10 μm) ilmenite-hematite crystals are scattered in the glass together with scarce clinopyroxene and apatite. As in the undoped run, we detected in the peridotite high Na_2O and CaO orthopyroxene (opx2) in (nephelinitic) glass pockets and high Na_2O, Cr_2O_3 and low CaO neo-formed augitic and omphacitic clinopyroxene. High Cr# (0.64-0.65) spinels (sp2) are commonly present in the whole lherzolitic portion; their TiO_2 contents (1.2-1.8 wt.%) are greater than in sp1 and in sp2 of the undoped run. Furthermore, the Mg# (0.48-0.50) is the lowest among the analysed spinels in all experiments.

At 975°C some clinopyroxene, olivine and spinel crystals are scattered in the glass in the nephelinitic portions of the capsule. Some olivine (Fo_{90}) crystals probably coming from the lherzolitic portion are present in the lower nephelinitic section. Neo-formed clinopyroxene and spinel crystals are found in the (central) lherzolitic portion of the charge. In particular, cpx2 shows slight Na_2O enrichment (up to 1.53 wt.%) and CaO depletion (down to 20.7 wt.%) with respect to cpx1.

Nephelinite-wehrlite runs

At 1.0GPa nephelinite layer of anhydrous experiments is completely molten at 1250°C; at 1200°C olivine crystallises, joined by clinopyroxene at 1150°C and by spinel and nepheline at 1050°C. In the hydrous experiments performed at 1150°C and 1050°C, crystal assemblages in nephelinite are the same as the anhydrous experiments but lack nepheline; rhönite and apatite occur at lower temperature. It is evident that at different temperatures different melt composition start to interact with the wehrlitic layer and their composition are reported in Table 4c and shown in the classification TAS diagram (large symbols of Fig. 3a).

Melts are in contact with the wehrlite through a reaction area whose extent depends on experimental temperature and run duration. The influence of the experimental time is displayed by the replicated anhydrous experiment at 1150°C: in the shorter run (8 hours) the reactions are limited to a ~250μm wide area while in the long time run (24 hours) the reaction affects all the wehrlite layer.

Run at T = 1250°C

The wehrlite layer is strongly infiltrated and three sub-layers can be recognized (Fig. 2): in the boundary layer (I), 300μm wide closest to nephelinite melt, clinopyroxene (cpx1) dissolved completely resulting in a mush of olivine+melt (Fig. 2a). The melt composition in this region is controlled by the contribution of cpx1 dissolution in the nephelinite; the resulting melt is enriched in SiO_2, CaO and depleted in alkalis (mainly Na_2O), TiO_2 and P_2O_5 (Table 4; Figs. 3a-d). The mg# is close to that of nephelinite.

The olivine grains become more rounded or show embayed rims; the composition is depleted in iron (Fo=82.6) relative to primary olivine (Fo=80.8; ol1). Calculated partition coefficients ($K_{DMg/Fe}$) for Mg and Fe (all Fe as FeO) between olivine and the associated melt range from 0.23 to 0.26. - Highest $K_{DMg/Fe}$ approach the equilibrium values of 0.3±0.03 for mafic melts (Roeder and Emslie, 1970).

Layer (II), about 600μm wide, is composed by olivine, clinopyroxene and interstitial melt that may contain neocrysts of olivine and clinopyroxene (Figs. 2a,b). The melt fraction of this layer is very low relative to layer (I) and the glass occurs in interstitial patches rarely connected to olivine+melt layer by very thin veins. Neo-olivine crystallised in the largest glass blebs are subequant and up to 25μm in size whereas neo-clinopyroxenes are anhedral and similar in size to the neo-olivine. The primary crystals preserve as a whole their original shape, showing slightly rounded rims when occur near to the small glass blebs; sometimes original olivine close to the large blebs, show an overgrowth of neo-olivine (Fig. 2b).

The compositional variation observed in the primary phases consists in the enrichment of forsterite component in olivine (from ~Fo80 in ol1 to an average of Fo84.3 in ol2) and depletion in TiO_2, Al_2O_3, FeO and Na_2O, besides of increase of mg#, in clinopyroxenes (Table 4). These compositional changes indicate a restitic character for these crystals (Hirose and Kawamoto, 1995; Shaw *et al.*, 2006).

Compositions of the interstitial glass pools, reported in Table 4, differ significantly from glasses at the interface nephelinite-wehrlite ("boundary layer"). Moving towards layer III, as melt pools decrease in size, the compositions change displaying an increase in SiO_2, Al_2O_3, FeO and alkalis (Na_2O in minor extent) and a decrease of TiO_2, CaO, P_2O_5 and mg# (Table 4 and Fig. 3).

The secondary olivine (ol2) grown in the largest melt pools have similar composition to restitic olivine (an average Fo83.5) while secondary clinopyroxenes (cpx2) are enriched in TiO_2 (1.1-2.7 wt.%), Al_2O_3 (4.2-7.2 wt.%), FeO (6.2-10.4 wt.%) and Na_2O (1.0-1.6 wt.%) contents (Figs. 4a-c) with respect to cpx1 (Table 4). The mg# of cpx2 ranges from 66 and 74 (Table 4).

Restitic olivine has $K_{DMg/Fe}^{ol/liquid}$ between 0.03 and 0.19 while $K_{DMg/Fe}^{ol/liquid}$ between ol2 and the associated melt ranges from 0.14 to 0.17, all consistently lower than equilibrium values. Lowest $K_{DMg/Fe}^{o/liquid}$ are related to glass with the highest SiO_2 content. $K_{DMg/Fe}^{cpx/liquid}$ (all Fe as FeO) of restitic clinopyroxene falls out of the equilibrium range of 0.25-0.32 (Nielsen & Drake, 1979, Shaw *et al.*, 1998) being encompassed between 0.08 and 0.12. Conversely, the $K_{DMg/Fe}$ for cpx2 and melt pairs are close to equilibrium values ranging from 0.26 to 0.38.

In the layer (III), the most distal from nephelinite/wehrlite interface (Fig. 2a), olivine and clinopyroxene have compositions similar to those of "restitic" crystals in layer II but fractions of secondary melt are very low and are not large enough to be analysed.

Runs at T < 1250°C

As in the 1250°C run, the wehrlite layer shows various degree of interaction with infiltrated melts. In all experiments the boundary layers (on average 250μm wide) are characterised by the high melt fraction; the reaction between liquid and wehrlite results in a decrease of clinopyroxene abundance and growth of neo-formed olivine, which occurs either as discrete grains or rims on the original crystals. In the remaining wehrlite, the infiltrating melt forms small patches or a network of thin veins and interstitial glass pools spreading across the entire wehrlite layer. In the short duration (8-hours) experiment at 1150°C the melt-rock interaction area is restricted to a narrow area (about 100μm area).

Minerals

The neo-formed olivine crystallised at the boundary layer is depleted in the Fo component with respect to ol1, approaching the composition of olivine crystallising in the nephelinite area (from ol2=Fo76 at 1200°C to ol2=Fo61 at 1050°C; Table 4). Dissolution of initial clinopyroxene in this region strongly decreases from the experiment at 1200°C to the 1050°C run.

In the wehrlite, primary olivine and clinopyroxene do not show significant textural variations and olivine neocrysts may grow in the largest melt pools. The olivine neocrysts progressively approach the composition of ol1 (Table 4). Original clinopyroxene (cpx1) develops narrow (up to 50μm) and irregular reaction rims (cpx2; Fig. 2c) enriched in TiO_2 (up to 1.25 wt.% at 1200°C; up to 5.55 wt.% at 1050°C), Al_2O_3 (up to 5.4 wt.% at 1200°C; up to 8.9 wt.% at 1050°C), FeO (up to 6.5 wt.% at 1200°C; up to 9.2 wt.% at 1050°C) and Na_2O (0.8 wt.% at 1200°C; up to 1.4 wt.% at 1050°C). These enrichments are coupled with decreasing mg# values (Table 4 and Figs. 3a-d) (see also Shaw *et al.*, 2006 and references therein). It is noteworthy that the cpx2 compositions of each experimental run are related to the composition of the reacting melt, which in turn, depends on the experimental temperature (Fig. 3e). Some of the scatter observed inside each compositional trend is due to the irregular extent of the melt/rock reactions (Fig. 2c).

In the hydrous experiments at 1150°C and 1050°C, cpx1 dissolution at the interface with the melt is reduced with respect to the anhydrous counterparts. A few amount of cpx1 dissolved completely (at 1150°C) or partially (at 1050°C) in an area about 200micron wide (Figs. 2e,f). The neo-formed phases found both at the interface and inside the wehrlite layer, show the same kind of compositional modifications and textural features recognized in the anhydrous experiments (Figs. 4a-c). In the 1050°C run a Ti-rich spinel also crystallises at the boundary layer (Fig. 2f).

Glasses

A network of melt veins and/or interstitial glass pools is observed in all the experiments. This is connected to the nephelinite. Melt compositions of the analysable glass are reported in Table 4.

In the 1200°C and 1150°C experiments, including the longest duration run at 1150°C, most of the interstitial pools resulted too small to be analysed. Glasses analysed at the boundary layer show weak chemical modifications with respect to nephelinite, except than

for alkalis (mainly Na_2O) that resulted enriched in the experiments at 1150°C. The same enrichment was not observed in glasses from 1200°C run, which chemical features rather record the higher contribution of clinopyroxene dissolution (Tab. 4; Fig. 3a-f).

In the hydrous and anhydrous experimental runs performed at 1050°C, the melts occurring at the boundary layer and invading wehrlite have the most differentiated compositions (Fig. 3a), being derived by high degrees of nephelinite crystallisation at this temperature; travelling inside the rock, these melts shows an increase in SiO_2 (up to 55%) and K_2O (up to 4.5%) and a depletion in CaO, P_2O_5 (not shown), and TiO_2 (although these last two elements display an increase at the top of wehrlite, Fig. 3c). In these runs, Na_2O content in the melts patches is influenced by the presence of water that prevented the nepheline crystallisation in the hydrous nephelinite-derived melt; as a consequence, Na_2O concentrations in wet experiments are higher than in anhydrous ones, reaching 10wt% in the distal interstitial patches. Similar Na content is attained in the water-free runs only in the melt portions that exist along the wall of the graphite capsule (Fig. 3e).

It is worth noting that the variation of mg# values has a good covariance with SiO_2 (not shown).

In terms of mineral/melt Mg and Fe exchange equilibrium we found that olivine $K_{DMg/Fe}^{ol/liquid}$ (0.27-0.33) and clinopyroxene $K_{DMg/Fe}^{cpx/liquid}$ (0.2-0.28) in the boundary layer approach equilibrium values for the highest temperature experiment (1200°C) or the longest duration runs (1050°C - 48 hours). In the wehrlite layer the $K_{DMg/Fe}^{ol/liquid}$ are generally lower (0.15 – 0.18) than those calculated for the boundary layer, even if $K_{DMg/Fe}^{cpx/liquid}$ shows a very wide range (0.12-0.35) with most falling in the range 0.24-0.30 indicating equilibrium between most of clinopyroxenes and associated melts. The low K_D values for olivine may be due to the high SiO_2 content of the glass occurring in this area (Draper & Green, 1997; Show *et al.*, 1999).

$K_{DMg/Fe}^{phases/liquid}$ computed for 1150°C experiments are constantly low (<0.19 and <0.18 for olivine and clinopyroxene respectively). These low K_D are not linked to the occurrence of high SiO_2 melts and may be related to run duration too short to attain equilibrium.

DISCUSSION

The ubiquitous occurrence of neo-formed clinopyroxene and spinel in the lherzolite and clinopyroxene and olivine in the wehrlite, indicate that both underwent a chemical modification at the experimental condition.

The modifications observed in lherzolite and wehrlite will be hereafter discussed.

Nephelinite/lherzolite reaction

The distribution and the paucity of the glass do not allow a reaction front to be clearly identified in the lherzolitic portion of the charges. This can be ascribed to a fast kinetics of the melt infiltration process that comes to early completion even in the shortest run, as a consequence of the low viscosity of nephelinite derived melts. This affects the spatial distribution and chemical composition of the neo-formed phases that do not show regular compositional variations from the lherzolite/nephelinite interface to the internal parts of the peridotite.

Neo-formed minerals (cpx2, sp2) could form either from partial melting process of lherzolite or from metasomatic reactions. However, the chemical variations recorded in cpx2 are not compatible with partial melting (e.g., see their Na_2O and Al_2O_3 content) and although the Cr# increase from sp1 to sp2 could be due also to partial melting (e.g.: Matsukage & Kubo, 2003), the fact that Cr# variations are unrelated with T of experiments rules out this hypothesis. Moreover, an increase of Cr# in spinels is reported to occur as a result of metasomatic reactions in lherzolite (e.g.: Francis, 1976; Neal, 1988; Sen & Dunn, 1994). In addition, the fact that TiO_2 content in sp2 increases if a Ti-doped nephelinite is used clearly indicates that neo-formed phases result from interaction with the alkaline melt. Textures observed in lherzolite for neo-formed phases point to rock-melt interaction. In particular, the occurrence of cpx2 together with glass in association with orthopyroxene (and olivine) is reported to be a consequence of orthopyroxene interaction with silica undersaturated melts (Shaw *et al.*, 1998, Shaw, 1999). Moreover, sp2 coronas observed around original spinel crystals closely resembles those reported by Shaw *et al.* (2006) in mantle peridotite xenoliths that underwent interaction with silica undersaturated melts.

The main compositional features of cpx2 and sp2 can be compared with those of natural phases thought to be a consequence of reaction with metasomatising melts. In Figures 5 and 6 composition of neo-formed clinopyroxene and spinel in the lherzolitic portion of the capsule are given together with that of original phases in lherzolite 154L. Furthermore,

clinopyroxenes from unmetasomatised xenoliths and clinopyroxene associated with amphibole (cpx-A) and secondary clinopyroxenes (i.e. in the reaction rim of orthopyroxene, cpx2-O) studied by Coltorti *et al.* (2004) are also reported for a comparison.

The higher Na_2O contents and the concomitant increase in Al_2O_3 and Cr_2O_3 (Fig. 5) of cpx2 synthesised at 2 GPa is a result of the entrance of trivalent cations (Al, Cr, Fe) in the M1 site due to the decrease in cell volume at increasing P. Such a high Na_2O increase is not observed in crystals formed at 1.5 GPa and in natural lherzolitic samples in which cpx-A coexists with pargasitic amphibole (containing ~ 3 wt.% Na_2O).

The Cr_2O_3 contents in cpx2 are comparable with those of cpx-A while cpx2-O shows contents similar to some cpx2 formed at 1150°C. MgO enrichment (Fig. 5), associated with CaO depletion occurs in the experimentally produced clinopyroxenes but not in cpx-A.

The SiO_2/Al_2O_3 versus TiO_2 diagram has been used by Coltorti *et al.* (2004) to show the chemical variations of both cpx-A and cpx2-O. In particular, according to these authors, TiO_2 in cpx-A approaches 6 wt.% (Fig. 5). Some cpx2 crystals (formed at 2 GPa) show TiO_2 enrichments up to 1 wt.% while SiO_2/Al_2O_3 ratios of cpx2 formed at low T (especially at 1150°C) approach those of cpx2-O.

In summary, cpx2 chemistry does not match that occurring in natural samples, although SiO_2/Al_2O_3 ratios detected in cpx2-O (from natural metasomatised lherzolites) is approached by some cpx2 synthesised at low T.

For spinel, Cr# and Mg# appear to be inversely correlated and TiO_2 content approach 2.0 wt.% in runs performed using the Ti doped starting material (Fig. 6). No worthwhile comparison can be drawn between these findings and the data reported by Coltorti *et al.* (2004) due to the paucity of the analytical data for spinels reported by these authors. However, it can be noted that a general Cr# and TiO_2 increase and a slight Mg# decrease was also observed in natural sp2 (Fig. 6).

Finally, analyses of glass obtained at 1250°C, approach the composition of some Si-rich glasses found in xenoliths where the interaction involving orthopyroxene occurs (Shaw *et al.*, 1998; Shaw, 1999). In the discrimination diagram $CaO+ Na_2O$ vs. $TiO_2+ K_2O$ proposed by Coltorti *et al.* (2000) to identify the nature of the metasomatic agents, these glasses plot in the field pertaining to metasomatism caused by Na-alkaline silicate melt.

Nephelinite/wehrlite reaction

The effect of metasomatic reactions recognised in the wehrlite/nephelinite experimental runs were compared with those observed in metasomatised wehrlites and pyroxenites from Browning Pass, Baker Rocks and Mt. Overlord, (NVL), Antarctica. These metasomatised rocks, both amphibole-free and amphibole-bearing, are interpreted to be the result of successive infiltration of rising alkaline melt(s) into pyroxenite bodies formed by a fractionation process at different condition of pressure and temperature (Perinelli & Armienti 2005).

The compositional features recorded by clinopyroxene in our experiments reveal the most representative effects of the reactions with the infiltrating melt. The differences between original and secondary clinopyroxenes, and the comparison of these latter with the cpx2 in natural samples are evaluated on the basis of their TiO_2, Na_2O, SiO_2, Al_2O_3 contents and mg#, resulted to be the most distinguishable chemical parameters. Experimental neo-clinopyroxenes define a trend of decreasing SiO_2/Al_2O_3 with increasing TiO_2, from the less to the more reacted crystals (Fig. 4a); these last overlap the trend defined by neo-clinopyroxenes in natural metasomatised pyroxenites (Fig. 4a). The enrichment of TiO_2 in experimental cpx2 is also associated to the increase of FeO content that, in terms of mg#, shows a trend similar to that of natural cpx2 although these last display a more limited mg# variation (Fig. 4b). It is noteworthy that in the area of experimental boundary layer, the distribution of TiO_2 and FeO enrichments along the reaction rims surrounding primary clinopyroxenes may be not correlated. For instance, the clinopyroxene shown in Figure 2f, has similar mg# (point A mg# = 68.9 and point B mg# = 68.3) along all reaction rim and results in equilibrium with the adjacent melt in term of $K_{DMg/Fe}^{cpx/liquid}$ (0.24 and 0.25 respectively), but the TiO_2 content is very different (point A TiO_2=5.33 wt% and point B TiO_2=2.49 wt%). This may be due to the different diffusive rate of these elements and to the amount of glass adjoining the crystal: the higher diffusive velocity of Fe (and Mg) with respect to Ti, allow to reach the crystal/liquid equilibrium also when the amount of adjacent glass is low; when the clinopyroxene borders large melt pools and the crystal can grow, the new composition approaches that of clinopyroxenes crystallised in the nephelinite area that show very high TiO_2 content (up to 6 wt%).

The mutual variation of Na_2O and Al_2O_3 of experimental cpx2 follows a smooth positive trend that includes also some natural secondary clinopyroxenes found in the metasomatised amphibole-free pyroxenites. Most of natural cpx2, instead, define a steeper trend with a

slight (or no) Na_2O increase (Fig. 4c). These natural cpx2 occur almost all in amphibole bearing samples suggesting that the crystallisation of amphibole may affect the Na_2O behaviour in clinopyroxene. Sen and Dunn (1994) in their experimental work concerning melt/lherzolite interaction observed a similar relationship between amphibole crystallisation and Na_2O content of associated clinopyroxene.

In this framework, the compositional modifications recorded by clinopyroxene in our reaction experiment on wehrlite, are alike those observed in experimental and natural mantle rock/melt systems where the reactions involves high melt/rock volume ratio (e.g. Sean & Dunn, 1994; Shaw *et al.*, 1998; Shaw, 1999; Coltorti *et al.*, 2004; Perinelli *et al.*, 2006; Shaw *et al.*, 2006; § "Nephelinite/lherzolite reaction" of this paper). The occurrence of amphibole, therefore, seems to be the sole parameter affecting the compositions of secondary pyroxenes in the variously metasomatised mantle rocks.

Glasses

All the glasses represent melts generated from the nephelinite. The temperature dependent path of nephelinite-derived melts is illustrated in the basalt tetrahedron CaTs-Di-Ol-Q pertaining to the CMAS system (Fig. 7). Nephelinite-derived compositions lay on an olivine control-line down to 1150°C; at lower temperature clinopyroxene crystallisation drives the metasomatising melts towards a phono-tephritic composition. At the different temperatures, these are the melts that are provided to the boundary layer and start infiltration (Fig. 7).

The processes that affect the nephelinite-derived melts at the very boundary layer are themselves evident in the pseudo ternary projection from quartz (Q) component of the basalt tetrahedron CaTs-Di-Ol-Q of Fig 7. Boundary-layer melts from higher T anhydrous experiments (1250°C-1150°C), are influenced to a different extent by the effect of the preferential dissolution of primary clinopyroxene that imply an increase in the abundance of cpx-derived oxides, SiO_2 and CaO (see Fig. 3). Melts from 1150°C hydrous run reveal, with respect to its anhydrous analog, a negligible contribution of cpx1 dissolution and a significant crystallization of both secondary olivine and clinopyroxene. Similarly, boundary layer melts of lower-temperature runs (1050°C), when anhydrous, show a very low assimilation of primary clinopyroxene, when hydrous, they show essentially the crystallization of neo-formed olivine + clinopyroxene. These 1050°C glasses, hydrous and anhydrous, display a rise in alkalis and a decrease in calcium contents (Fig. 3).

The control of assimilation/crystallisation processes on the composition of boundary layer melts in both hydrous and anhydrous runs, is evidenced in more detail in the small triangles of Fig. 7. They show that cpx1 dissolution has a significant role for anhydrous experiments, whereas in hydrous runs, the compositional effect on the glasses of cpx1 assimilation may be hidden by the contemporaneous crystallisation of neo-crystals of the same phase. Moreover, all boundary layer melts are affected by olivine crystallisation. A cursory inventory of olivine and clinopyroxene amounts involved in the formation of boundary layer melts may be performed with the diagram in Figure 7 applying the lever rule. For anhydrous melts, at 1250°C, up to 15% of olivine crystallization is necessary together with consistent (up to 40%) clinopyroxene assimilation. At lower temperature much lower amount of olivine crystallization (0-5%) and clinopyroxene assimilation (10%) are required. For hydrous melts olivine and clinopyroxene crystallisation always occurs. Note that the amount of glass is very low and the above percentages do not imply a large amount of melting of the original paragenesis.

Boundary layer melts thus appear to be controlled by clinopyroxene dissolution and/or crystallisation in a way that can be recognized as a reaction front (Lundstrom, 2003; Morgan & Liang, 2003).

When boundary layer melts migrate through the wehrlite, they change in composition due both to the nucleation of new phases and reaction with pre-existing clinopyroxene and olivine. As a consequence, they progressively enrich in SiO_2, Al_2O_3 and alkalis and deplete in TiO_2 and P_2O_5 (Fig. 3). However, the observed trends in Harker's diagrams (Fig. 3 and inset in Fig. 7) seem to indicate that also a diffusive flux of Na_2O and K_2O occurred from nephelinite-wehrlite boundary layer into wehrlite; the interstitial pools are thus enriched in the faster diffusing elements (Na_2O and K_2O) with respect to the slower diffusing TiO_2 and P_2O_5, according to a process well documented in other experimental studies ("uphill diffusion" of Shaw *et al.*, 1998, see also Lundstrom, 2003; Morgan & Liang, 2003 and references therein). The competing behavior between the two differently diffusing TiO_2 and Na_2O is evident considering that the continue clinopyroxene/melt interaction in wehrlite should reduce sodium and titanium content in the melt due to their absorption by clinopyroxene, instead TiO_2 displays the expected trend while Na_2O increases (Fig. 3).

The continue clinopyroxene/melt interaction in fact should change in the same way both Na_2O and TiO_2 and the decoupling of these two elements shown in Fig. 3 could be explained by their different diffusivity. Moreover, the differences in the Na_2O-SiO_2

enrichment trends, shown by wet and dry experiments at 1050°C, underline the strong effect of water on the alkali diffusivity (Freda & Scarlato, 2001 and references therein).

Finally, the highest Na content attained in the water-free runs found in the melt portions along the wall of the graphite capsule may be explained with a melt advection process (Lundstrom, 2003).

Although chemical transport by diffusion may have some role on glass compositions, the different behaviour of the elements in experimental melts mainly depends on melt/rock ratio (Navon & Stolper, 1987; Bodinier *et al.*, 1990; Bedini *et al.*, 1997; Vernières *et al.*, 1997 and Ionov *et al.*, 2002). For high melt/rock ratio conditions, the compositional modification of the reactant liquid is prevented or limited to a thin layer at melt-rock boundary (nephelinite-wehrlite interface). Low melt/rock ratios cause progressive compositional changes of percolating melt due to its continuous interaction with the rock assemblage. Therefore, the compositional variations of infiltrating melts and reacted phases are a function of the distance from the melt source, i.e. from the nephelinite layer and depend on the rate of melt infiltration in addition to the reaction processes.

The compositions of experimental glasses, when compared with those of natural samples reveal some significant similarities: in particular, the alkali-rich melt compositions from hydrous and anhydrous runs at 1050°C, mimic the alkali-rich glasses found in natural metasomatised amphibole-free pyroxenites (Fig. 3b-e). This suggests that in evolved T-X systems such as those experimentally reproduced at the lowest temperature, the compositions of melts probably were not suitable to form amphibole. Moreover, water content could have hindered amphibole nucleation; in fact, in spite of water addition in the 1050°C run, the metasomatised assemblage contains only some spinel, a phase that precedes amphibole nucleation in systems with low water activity (King et al., 2000).

Melts from runs at 1200°C, and interstitial melts at 1250°C approach natural low-alkali melt compositions (Fig. 3a) associated to amphibole-bearing pyroxenites, even if amphibole is absent in the experiments.

Lack of amphibole among experimental products

Amphibole, is a phase that directly reveals metasomatism on mantle rocks and occurs in many mantle xenoliths from NVL. In our experiments, amphibole was not detected, both in lherzolite and wehrlite. This was expected in high T experiments (T>1100°C); in lower T

runs amphibole formation could have been hampered by some parameters controlling its P-T stability field in mantle rocks, such as bulk rock composition, particularly alkali and Ti contents in lherzolite, and water content (e.g. Wallace & Green, 1991, Niida & Green, 1999). However, considering for comparison Sen & Dunn (1994) reaction experiments, it can be observed that, although they used an amphibolite-derived melt as metasomatising agent, amphibole nucleated as small (1-10 μm) grains, only at 975°C (and not at 1025°C) at the same P of our experiments (2.0 GPa).

A further parameter that may have hindered the amphibole cristallisation is the melt/rock ratios in the experimental charges that, as pointed out by Rapp *et al.* (1999), can affect the nature of chemical reactions and thus the mineralogy of the resulting assemblages.

Finally, although amphibole is out of its stability field at T > 1100°C, nonetheless, we noted that in the wehrlite/nephelinite system, the composition of melts from high temperature runs approaches natural melt compositions associated to amphibole-bearing pyroxenites. This lead us to consider that the lack of amphibole in the runs might be due to the experimental configuration; it imposes, in fact, a constant T to the system a condition that does not reproduce exactly the condition of the natural environment where a hot metasomatising melt infiltrate a colder matrix. Therefore, high-T experimental melts could represent suitable precursors of melts able to form amphibole, but to crystallise this phase it should infiltrate a matrix at lower temperature, which is excluded by the configuration of the experiments.

Relying upon these evidences, it is possible to consider that in the mantle, where a nephelinitic magma like SAX20 at 1200°C passes through a relatively cool wehrlite (850-1050°C; Perinelli & Armienti, 2005, Perinelli *et al.*, 2006), at the magma-wall rock contact, the wehrlite undergoes a transient heating such to induce clinopyroxene dissolution. The resultant melts, enriched in clinopyroxene components, may percolate into cooler wall rock while reacting with the wehrlitic mineral assemblage. Moreover, during their migration, melts crystallise secondary clinopyroxene and they progressively enrich in water just to achieve amphibole saturation. Similar processes, that can be accounted for in terms of "wall-rock" metasomatism and "diffuse" metasomatism (Xu & Bodinier, 2004 and references therein), probably lead to the amphibole crystallisation also into lherzolitic rocks, even if our experiments with lherzolite paragenesis did not provide any indication about these processes.

Our experiments, however, do not rule out the possibility that natural glasses associated to amphibole may be originated by interaction with a metasomatic agent different from SAX20 nephelinite (i.e. a low alkali and high TiO_2 hydrous liquid).

CONCLUDING REMARKS

Even if experiments on nephelinite/lherzolite-wehrlite assemblages did not produce amphibole, considerable chemical modifications are observed in both lherzolitic and wehrlitic portions of the charges. Moreover the runs show that compositional variations and their extent depend on melt/rock ratio and are a function of the distance from the melt source, i.e. from the nephelinite layer.

Clinopyroxene shows compositional variations in both lithotypes: it changes from diopside to high Mg-Cr-(Na) augites and omphacites in lherzolite and to low Mg and high Ti-Al-Fe-Na augites in the wehrlite. Its chemical variations partially fit the modifications of clinopyroxenes found in xenoliths and thought to be a result of reactions between a metasomatising melt as SAX20 and a lherzolite (wehrlite). In particular, we were able to reproduce experimentally at low T, the high SiO_2/Al_2O_3 ratios of secondary clinopyroxenes found as reaction rims of orthopyroxenes in lherzolite, whereas even the use of Ti-doped nephelinite did not cause the Ti increase observed in clinopyroxene of natural lherzolite. On the other hand, the Ti, Al and Na increase in natural clinopyroxenes of amphibole-free pyroxenites is quite well matched by crystals formed in wehrlite.

Furthermore, spinel (in lherzolite) and olivine (in wehrlite) were compositionally modified by metasomatic melts: Cr# increases and Mg# decreases in spinel, while forsterite decreases in olivine.

Nephelinite/lherzolite experiments produced scarce interstitial glass; the only analysable patches, from the 1.5GPa-1250°C experiment, have compositions that approach some melts related to orthopyroxene/melt reaction found in natural xenoliths. On the contrary, experiments on nephelinite/wehrlite system provided a variety of melts that fit in some extent the natural glasses. In particular, the runs at T<1150°C produced melts that mimic the trends shown by high-alkali and low-TiO_2 glasses found in the amphibole-free natural pyroxenites. Boundary layer glasses of high temperature (T>1150°C) runs could be the precursor of glasses associated to amphibole-bearing pyroxenites. They are significantly

affected by primary clinopyroxene dissolution and simultaneous crystallisation of the neo formed phases. The missing amphibole nucleation in the experiments was probably due to the fact that the fixed temperature imposed by the experimental setting does not allow to meet a stability field for amphibole which, instead, can form in nature in an evolving T-X regime where a hot metasomatising melt infiltrates a colder matrix.

This mechanism can be identified with a moving reaction front that, though implying a relative low amount of melts, may induce widespread metasomatic effects in wide mantle region. The different metasomatic style recognized in NVL can be account for in term of a process like this where the infiltration of rising basaltic melts, which are also responsible for the formation of pyroxenitic lenses and dykes with variable thickness, modify the chemical and mineralogical mantle composition, as well its thermal regime (Armienti & Perinelli, 2007 in prep.). Such differently metasomatised mantle source is probably responsible for Cenozoic magmatism, although the role played by amphibole (and clinopyroxene) in the magma generation is still a matter of considerable debate.

ACKNOWLEDGEMENTS

We are grateful to C. Shaw and M. Toplis for their very constructive reviews. The authors thank M. Coltorti for helpful discussions and encouragement, F. Olmi, C. Petrone (CNR-IGG) and M. Serracino (CNR-IGAG) for help during EPM analyses and F. Colarieti and M. Tamponi for the assistance in SEM analyses.

REFERENCES

Allen, J.C. & Boettcher A.L. 1978. Amphibole in andesite and basalt: II. Stability as a function of P-T-fH$_2$O-fO$_2$. *American Mineralogist*, **63**, 1074-1087.

Ballhaus, C.G., Berry, R.F. & Green, D.H. 1990. Oxygen fugacity controls in the Earth's upper mantle. *Nature*, **348**, 437-440.

Beccaluva, L., Coltorti, M., Orsi, G., Saccani, E. & Siena, F. 1991. Nature and evolution of subcontinental lithospheric mantle of Antarctica: evidence from

ultramafic xenoliths of the Melbourne volcanic province (northern Victoria Land, Antarctica). *Memorie della Società Geologica Italiana*, **46**, 353-370.

Bence A.E. & Albee A.L. 1968. Empirical correction factors for the electron microanalysis of silicates and oxides. *Journal of Geology*, **76**, 382-402.

Bodinier, J.-L., Vasseur, G., Vernieres, J., Dupuy, C. & Fabries, J. 1990. Mechanisms of mantle metasomatism: geochemical evidence from the Lherz orogenic peridotite. *Journal of Petrology,* **31**, 597–628.

Bedini, R.M., Bodinier, J.-L., Dautria, J.-M. & Morten, L. 1997. Evolution of LILE-enriched small melt fractions in the lithospheric mantle: a case study from the East African Rift. *Earth and Planetary Science Letters*, **153**, 67-83.

Bohlen, S.R.B., Essene E.J. & Boettcher A.L. 1980. Reinvestigation and application of olivine-quartz-orthopyroxene barometry. *Earth and Planetary Science Letters*, **47**, 1-10.

Carroll, M.J. & Wyllie, P.J. 1989. Flowing granite in experimental micro-magma chamber at 1050°C, 15 kbar. *European Journal of Mineralogy,* **1**, 249-260.

Coltorti, M., Beccaluva, L., Bonadiman, C., Salvini, L. & Siena, F. 2000. Glasses in mantle xenoliths as geochemical indicators of metasomatic agents. *Earth and Planetary Science Letters,* **183**, 303-320.

Coltorti, M., Beccaluva, L., Bonadiman, C., Faccini, B., Ntaflos, T. & Siena, F. 2004. Amphibole genesis via metasomatic reaction with clinopyroxene in mantle xenoliths from Victoria Land, Antarctica. *Lithos*, **75**, 115-139.

Draper, D.S. & Green, T.H. 1997. P-T phase relation of silicic, alkaline, aluminous mantle –xenolith glasses under anhydrous and C-O-H fluid-saturated conditions. *Journal of Petrology*, **38**, 1187-1224.

Francis, D. M. 1976. The origin of amphibole in lherzolite xenoliths from Nunivak Island, Alaska. *Journal of Petrology*, **17**, 357-378.

Freda, C., Baker, D.R. & Ottolini, L. 2001. Reduction of water loss from gold-palladium capsules during piston-cylinder experiments by use of pyrophyllite powder. *American Mineralogist*, **86**, 234-237.

Freda, C. & Scarlato, P. 2001. La diffusione nei fusi silicatici. *In*: Quaderni di geofisica , C. J. & Norry, M. J. (eds) *Istituto Nazionale di Geofisica e Vulcanologia*, **14**, 1-23.

Ionov, D.A., Bodinier, J.-L., Mukasa, S.B. & Zanetti, A. 2002. Mechanisms and sources of mantle metasomatism: major and trace element composition of peridotite xenoliths from Spitsbergen in the context of numerical modelling. *Journal of Petrology*, **43**, 2219-2259.

Irving, A. J., Huang, W. L. & Wyllie, P.J. 1977. Phase relations of portlandite, calcium hydroxide and brucite, magnesium hydroxide to 33 kilobars. *American Journal of Science*, **277**, 313-21.

King, P.L., Hervig, R.L., Hollowaly, J.R., Delaney, J.S. & Dyar, M.D. 2000. Partitioning of $Fe^{3+/}Fe_{total}$ between amphibole and basanitic melt as a function of oxygen fugacity. *Earth and Planetary Science Letters*, **178**, 97-112.

Le Bas, M.J., Le Maitre, R.W., Streckeisen, A. & Zanettin, R. 1986. A chemical classifcation of volcanic rocks based on the Total Alkali-silica diagram. *Journal of Petrology*, **27**, 745-750.

Lundstrom, C.C. 2003. An experimental investigation of diffusive infiltration of alkalis into partially molten peridotite: implications for mantle melting processes. *Geochemistry Geophysics Geosystems*, **4**, 1-25.

Matsukage, K. & Kubo, K. 2003. Chromian spinel during melting experiments of dry peridotite (KLB-1) at 1.0-2.5 GPa. *American Mineralogist*, **88**, 1271-1278.

Morgan Z. & Liang Y. 2003. An experimental and numerical study of kinetics of harzburgite reactive dissolution with applications to dunite dike formation. *Earth and Planetary Science Letters*, **214**, 59-74.

Morimoto, N. 1989. Nomenclature of pyroxenes. *Canadian Mineralogy*, **27**, 143-156.

Navon, O. & Stolper, E. 1987. Geochemical consequence of melt percolation: the upper mantle as chromatographic column. *Journal of Geology,* **95,** 285-307.

Neal, C.R. 1988. The origin and composition of metasomatic fluids and amphiboles beneath Malaita, Solomon Islands. *Journal of Petrology*, **29**, 149-179.

Niida, K. & Green, D.H. 1999. Stability and chemical composition of pargasitic amphibole in MORB pyrolite under upper mantle conditions. *Contributions to Mineralogy and Petrology*, **135**, 18-40.

O'Hara, M. J. 1968. The bearing of phase equilibria studies in synthetic and natural systems on the origin and evolution of basic and ultrabasic rocks. *Earth Science Review*, **4**, 69-133.

Orlando, A., Armienti, P., Conticelli, S., Vaggelli, G. & Manetti, P. 1997. Petrological investigations on the primitive cainozoic lavas of Northern Victoria Land, Antarctica. *In*: *VII International Symposium on Antarctic Sciences, the Antarctic region: geological evolution and processes*, 523-529.

Orlando, A. & Borrini, D. 2001. Solubility of Ti in andradite under upper mantle conditions: preliminary results. *Periodico di Mineralogia*, **70**, 99-110.

Perinelli, C. & Armienti, P. 2005. Pyroxenites and megacrysts in alkaline basaltic magmas from northern Victoria Land (Antarctica): constraint on the thermal evolution of sub-continental lithosphere. *Ofioliti*, **30**, 231.

Perinelli, C., Armienti, P. & Dallai, L. 2006. Geochemical and O-isotope constraints on the evolution of lithospheric mantle in the Ross Sea rift area (Antarctica). *Contributions to Mineralogy and Petrology*, **151**, 245-266.

Rapp, R.P., Shimizu, N., Borman, M.D. & Applegate, G.S. 1999. Reaction between slab-derived melts and peridotite in the mantle wedge: experimental constraints at 3.8 GPa. *Chemical Geology*, **160**, 335-356.

Rocchi, S., Armienti, P., Di Vincenzo, G., Cardini, I., Rossetti, F., & Storti F. 2006. Tight link between Cenozoic magmatism and local-regional fault Activity in the West Antarctic Rift. *Terra Atartica Reports*, **12**, 73-80.

Rocholl, A., Stein, M., Molzahn, M., Hart, S:R., & Wörner, G. 1995. Geochemical evolution of rift magmas by progressive tapping of a stratified mantle source beneath the Ross Rift, Antarctica. *Earth and Planetary Science Letters*, **131**, 207-224.

Sen, C. & Dunn, T. 1994. Experimental modal metasomatism of a spinel lherzolite and the production of amphibole-bearing peridotite. *Contributions to Mineralogy and Petrology*, **119**, 422-432.

Shaw, C.S.J., Thibault, Y., Edgar, A.D. & Lloyd, F.E. 1998. Mechanisms of orthopyroxene dissolution in silica-undersaturated melts at 1 atmosphere and implications for the origin of silica-rich glass in mantle xenoliths. *Contributions to Mineralogy and Petrology*, **132**, 354-370.

Shaw, C.S.J. 1999. Dissolution of orthopyroxene in basanitic magma between 0.4 and 2 GPa: further implications for the origin of Si-rich alkaline glass inclusions in mantle xenoliths. *Contributions to Mineralogy and Petrology*, **135**, 114-132.

Shaw, C.S.J., Heidelbach, F. & Dingwell, D.B. 2006. The origin of reaction textures in mantle peridotite xenoliths from Sal Island, Cape Verde: the case for "metasomatism" by the host lava. *Contributions to Mineralogy and Petrology*, **151**, 681-697.

Ulmer, P. & Luth, R.W. 1991. The graphite-COH fluid equilibrium in P, T, fO_2 space; an experimental determination to 30 kbar and 1600 C. *Contributions to Mineralogy and Petrology*, **106**, 265-272.

Vaggelli, G, Olmi, F. & Conticelli, S. 1999. Quantitative electron microprobe analysis of reference silicate mineral and glass samples. *Acta Vulcanologica,* **11**, 297-303.

Vernières, J., Godard, M. & Bodinier, J.-L. 1997. A plate model for the simulation of trace element fractionation during partial melting and magma transport in the Earth's upper mantle. *Journal of Geophysical Research*, **102**, 24771-24784.

Xu, Y.,G. & Bodinier J.-L. 2004. Contrasting enrichments in high- and low-temperature mantle xenoliths from Nushan, Eastern China: results of a single metasomatic event during lithospheric accretion? *Journal of Petrology*, **45**, 321-341.

Zipfel, J. & Wörner, G. 1992. Four- and five-phase peridotites from a continental rift system: evidence for upper mantle uplift and cooling at the Ross Sea margin (Antarctica). C. *Contributions to Mineralogy and Petrology*, **111**, 24-36.

FIGURE CAPTIONS

Figure 1. Backscattered electron images of representative run products in lherzolite. **a**) run 170 (1250°C and 1.5GPa); **b**, **c**) run 169 (1150°C and 1.5GPa).

Figure 2. Backscattered electron images of representative run products in wehrlite. **a**) and **b**) run 141 (1250°C), **c**) and **d**) run 154 (1050°C) ad **e**) and **f**) run 154* (1050°C, wet run). I, II and III refers to different reaction areas observed in 1250°C run. cpx2 = clinopyroxenes produced by melt/rock reaction; ol restitic = olivine which suffered partial melting (1250°C). In **f) A** refers to the growth rim on primary clinopyroxene, and **B** refers to the reaction rim of the same crystal (see the text).

Figure 3. a) Experimental glasses from nephelinite/wehrlite runs plotted in the TAS classification diagram (Le Bas et al., 1986); **b**-**f**) compositional variations diagrams of experimental glasses. The arrows point out compositional variations resulting from the continuous interaction of infiltrating melts with the wehrlite. The large symbols represent the nephelinite-derived melts and "*" indicate the melt composition at boundary layer that starts infiltration. In the diagrams are also reported interstitial glasses occurring in natural wehrlites (grey area= amphibole-free pyroxenites, dashed grey area = amphibole-bearing pyroxenites; Perinelli & Armienti, in prep.).

Figure 4. TiO_2 vs. SiO_2/Al_2O_3 ratio **a**) TiO_2 vs. mg# **b**) and Al_2O_3 vs. Na_2O **c**) plots of synthesising clinopyroxenes in nephelinite/wehrlite experiments. In the diagrams are also reported secondary clinopyroxene related to metasomatism of natural wehrlites (grey area; Perinelli & Armienti 2005). The arrows in the upper right diagram indicate compositional variations induced by metasomatism on original clinopyroxene in function of distance from nephelinite/wehrlite boundary layer.

Figure 5. Diagrams showing composition of experimental (this paper) and natural clinopyroxenes from Coltorti *et al.* (2004). The legend is visualized in the upper left diagram. The shaded and the dotted areas represent the compositional field of cpx1

of lherzolite 154L (this paper) and cpx1 from Coltorti *et al.* (2004), respectively. The arrows in the upper right diagram point out compositional variations induced by metasomatism on cpx1, as reported by Coltorti *et al.* (2004).

Figure 6. Cr# vs. Mg# **a**) and Cr# vs. TiO_2 **b**) in experimental spinel. Legend as in Figure 5. The dotted arrows point out compositional variations induced by metasomatism on original spinels from mantle xenoliths (Coltorti *et al.* 2004).

Figure 7. Synthetic glasses plotted on pseudo ternary projection from quartz (Q) in the basalt tetrahedron CaTs-Di-Ol-Q pertaining to the CMAS system (O'Hara, 1968): C = (CaO - $3.33P_2O_5$ + $2Na_2O$ + $2K_2O$)* 56.08; M = (FeO + MnO + NiO + MgO – TiO_2)* 40.31; A = Al_2O_3 + Cr_2O_3 + Fe_2O_3 + Na_2O + K_2O + TiO_2)* 101.96; S = (SiO_2 - $2Na_2O$ - $2K_2O$)* 60.09 (all oxides in mol. prop.). Symbols as in Figure 3; ol1, cpx1 and cpx2 refer to primary olivine, clinopyroxene and secondary clinopyroxene, respectively. In the two smaller pseudo ternary projections are reported the trends of liquid evolution from the nephelinite-derived melts to interstitial melts for both anhydrous and hydrous experiments at the different temperature. The effect of alkali diffusion on the liquid compositions is evidenced in the inset SiO_2 vs. Na_2O diagram. From this diagram is evident that the glasses at the boundary layer of anhydrous experiments are affected by clinopyroxene dissolution mainly in the runs at the highest temperature. In the hydrous runs the clinopyroxene dissolution had negligible effect. In all experiments, the composition of melts formed into wehrlite is controlled by crystallisation of new olivines and clinopyroxenes besides of by alkali diffusion process.

TABLE CAPTIONS

Table 1. Representative composition of minerals in lherzolite and in wehrlite together with whole rock composition of nephelinite SAX20 and other synthetic starting materials used in the runs. Metasomatising melts inferred by Coltorti *et al.* (2004) are also reported for comparison.

Table 2. Experimental assemblage, run conditions and results.

Table 3. Representative electron microprobe analyses of cpx2 (**a**), sp1 and sp2 (**b**) and glasses (**c**) in lherzolite.

Table 4. Representative electron microprobe analyses of ol2 (**a**), cpx2 (**b**) and glasses (**c**) in wehrlite.

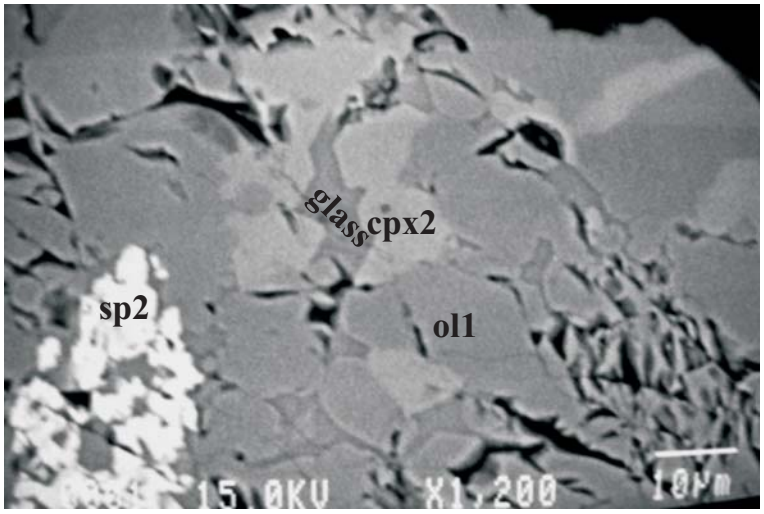

a)

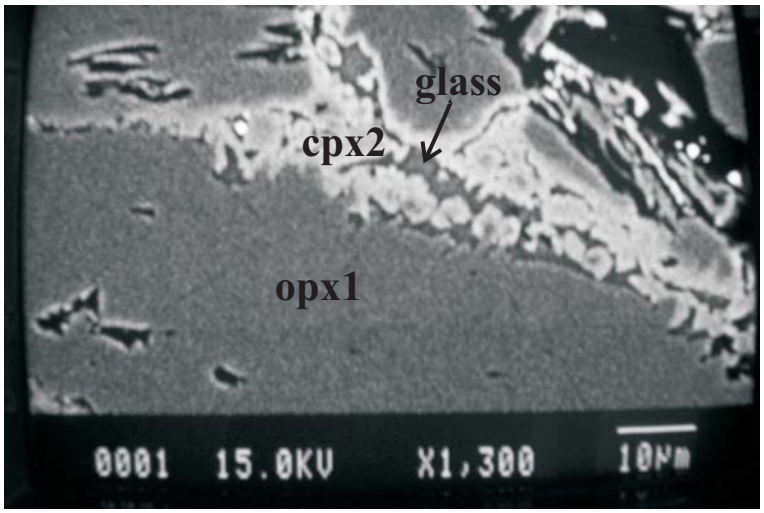

b)

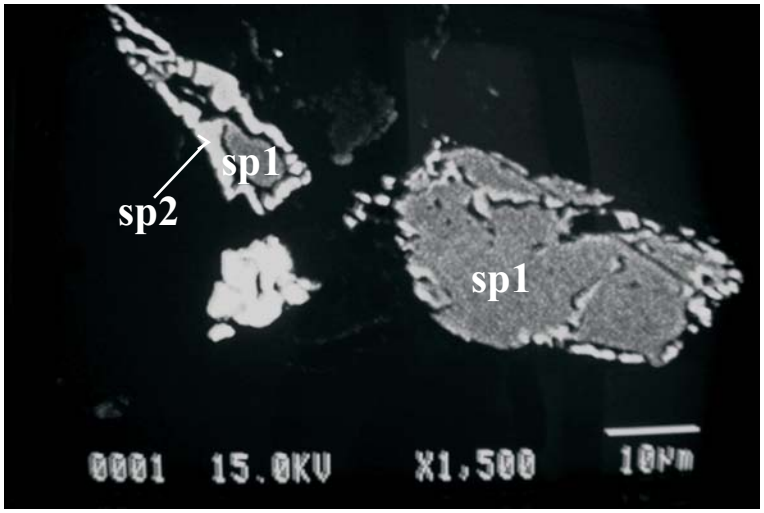

c)

Perinelli et al. Figure 1

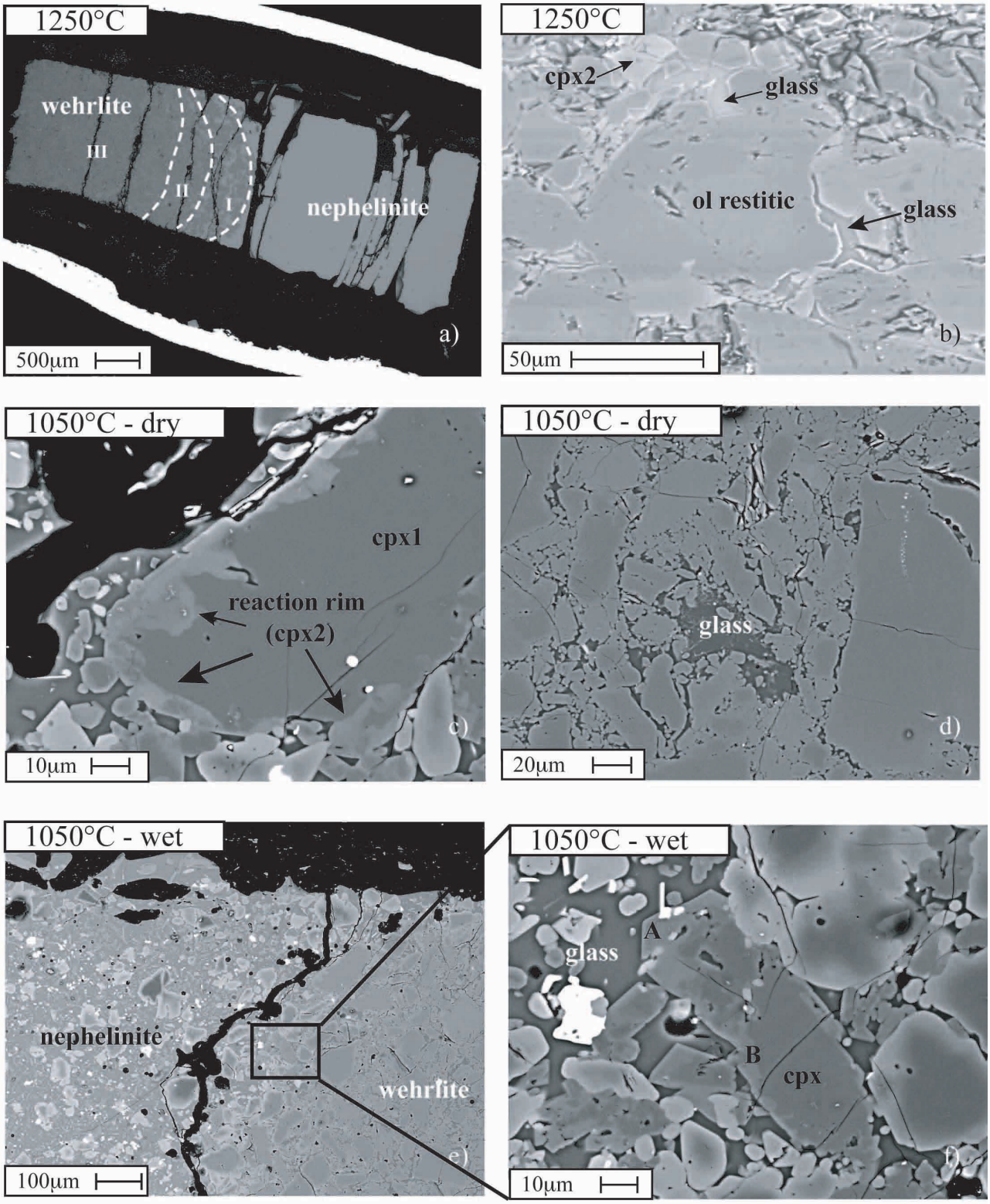

Fig. 2

Perinelli et al.

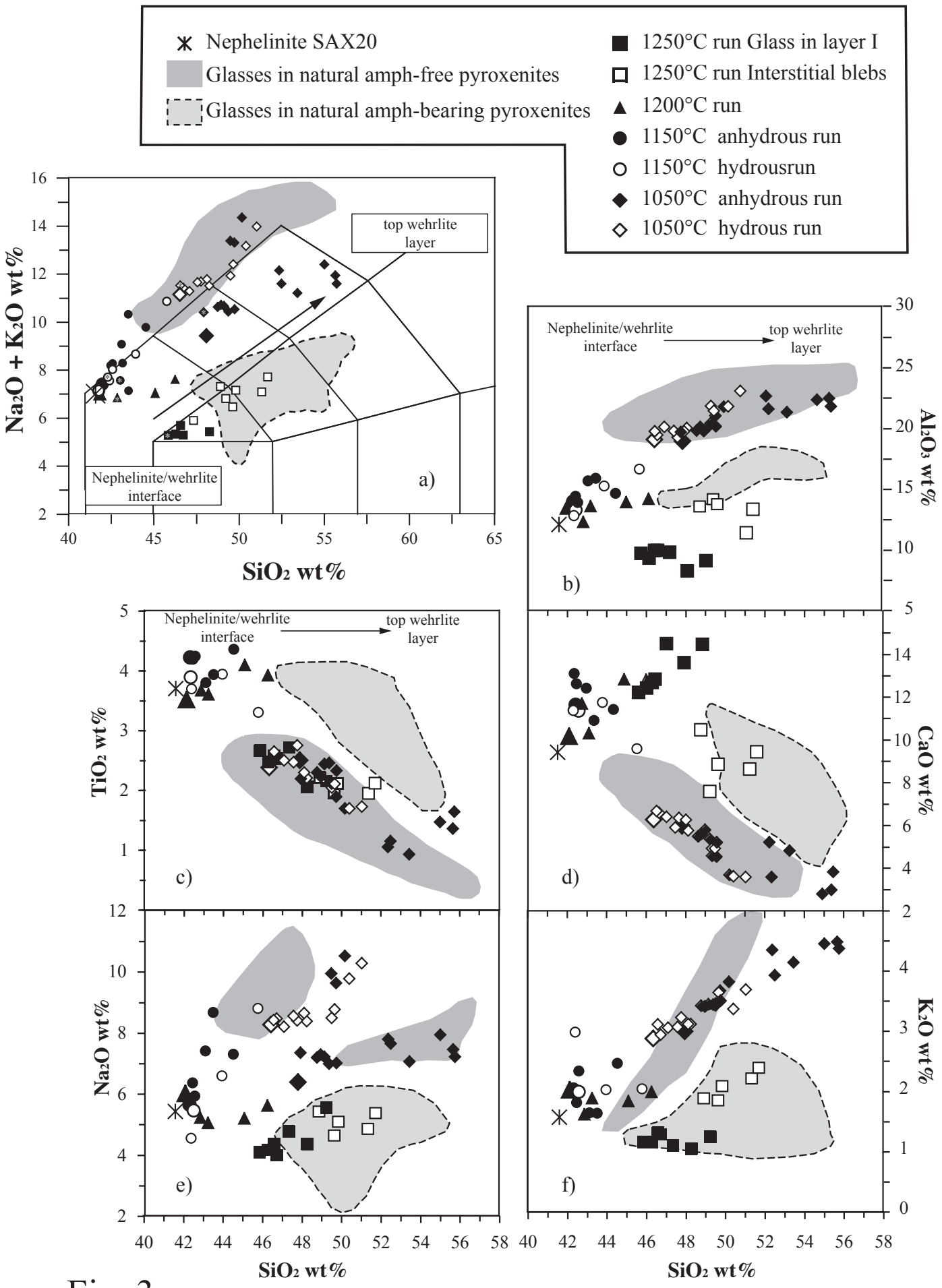

Fig. 3

Perinelli et al.

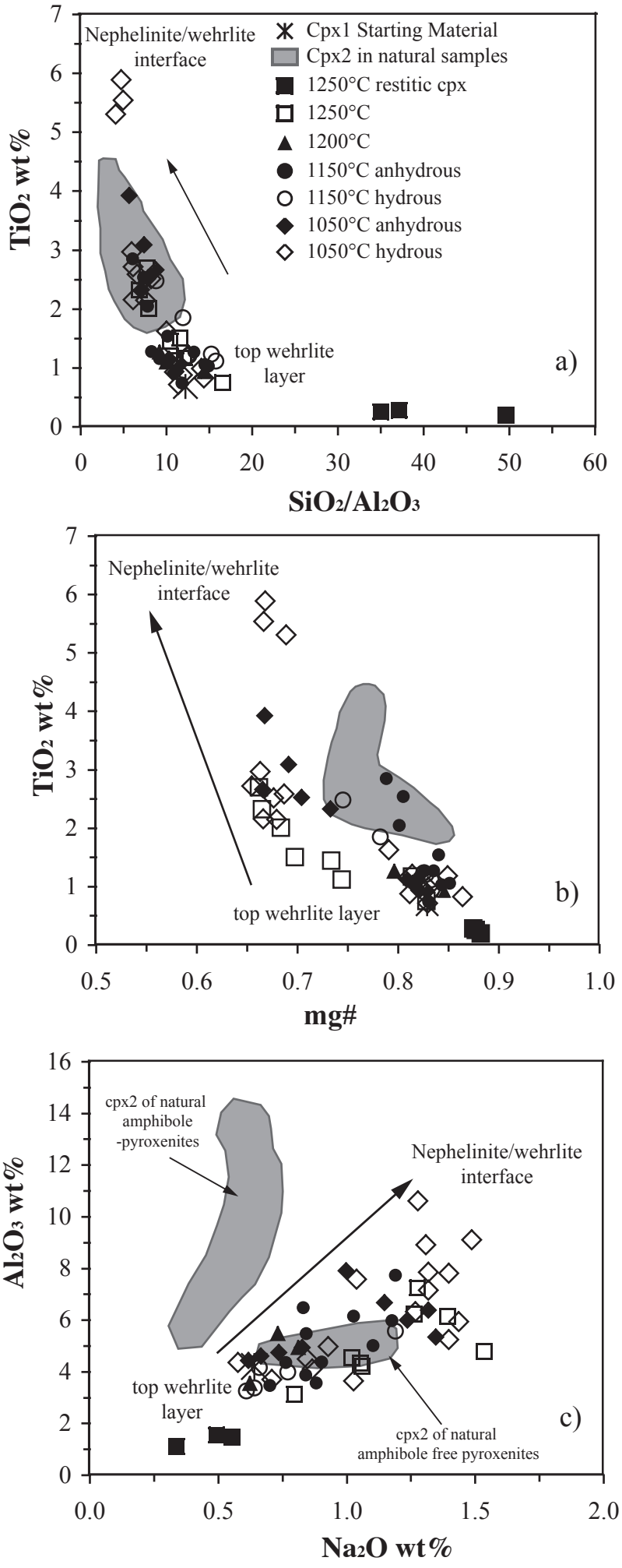

Fig. 4

Perinelli et al.

Clinopyroxenes in lherzolite

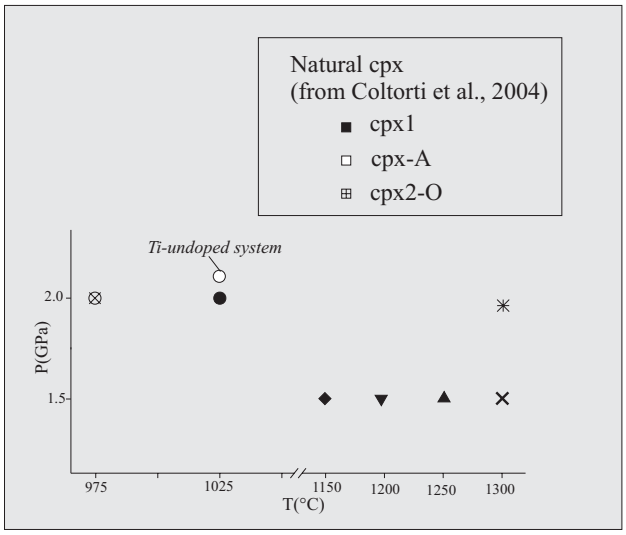

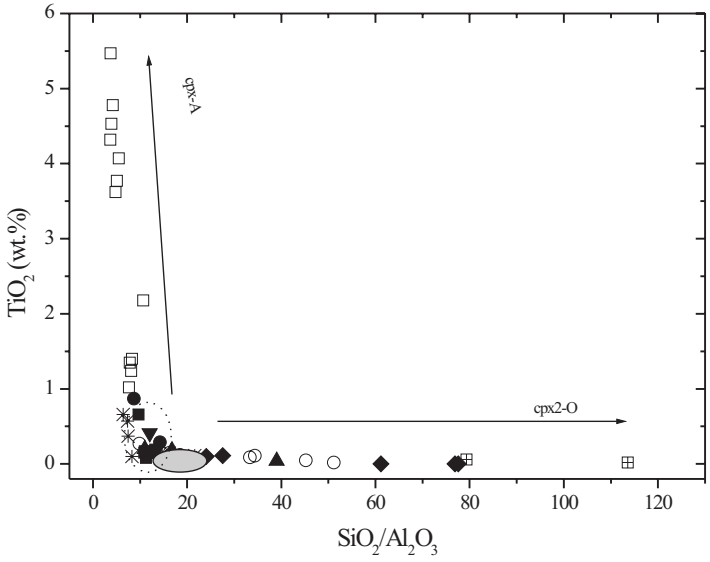

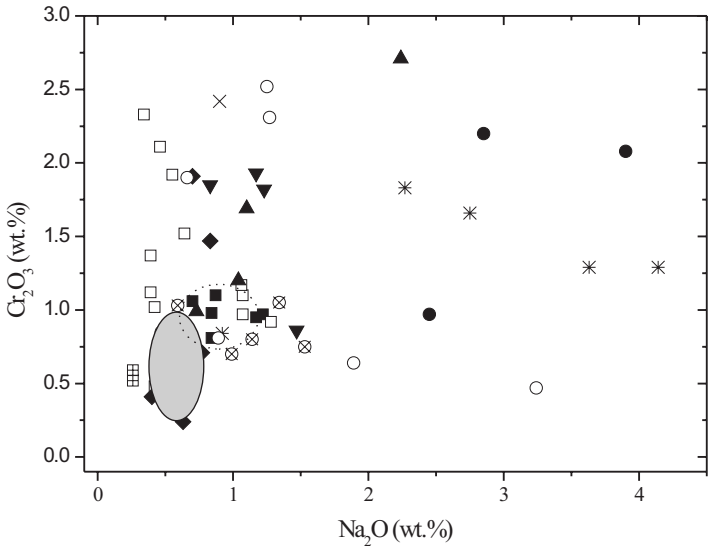

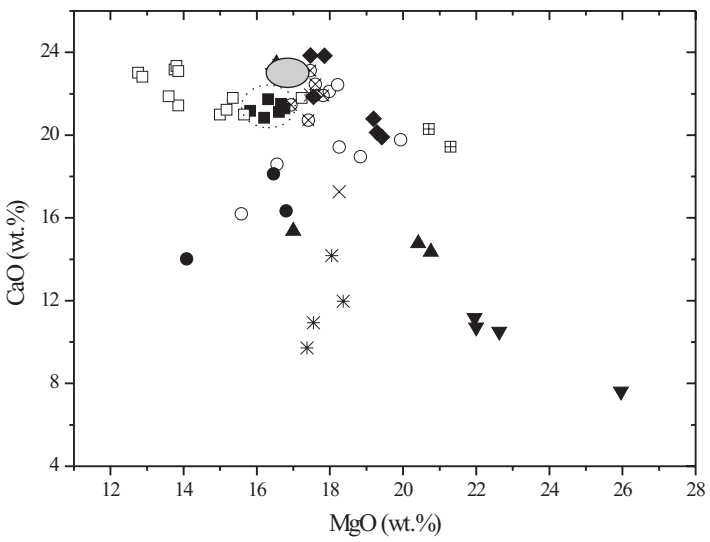

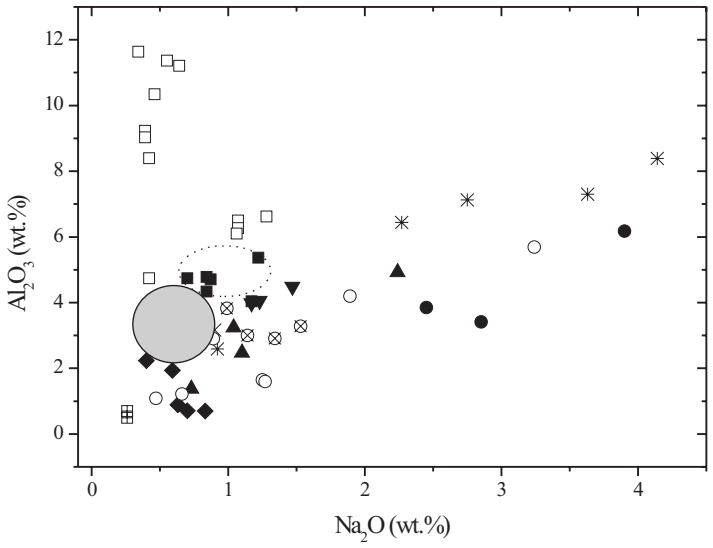

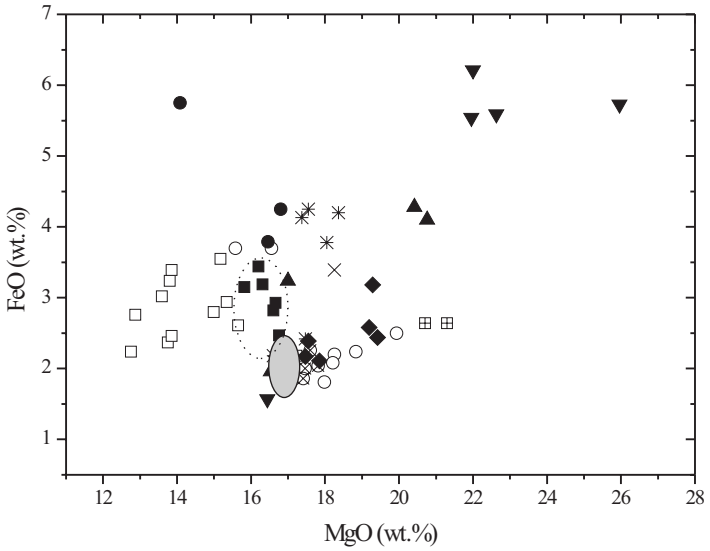

Perinelli et al., 2006 Figure 5

Spinels in lherzolite

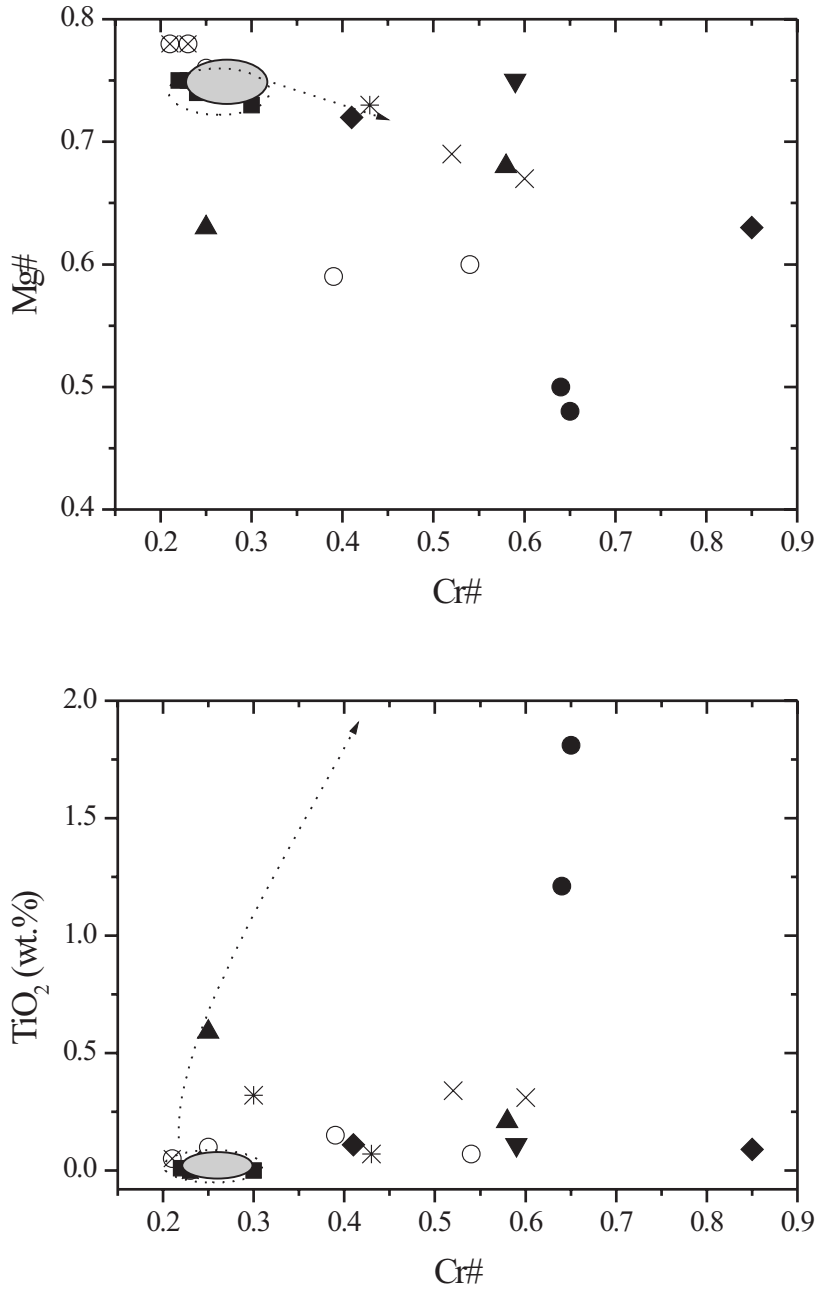

Perinelli et al., 2006 Figure 6

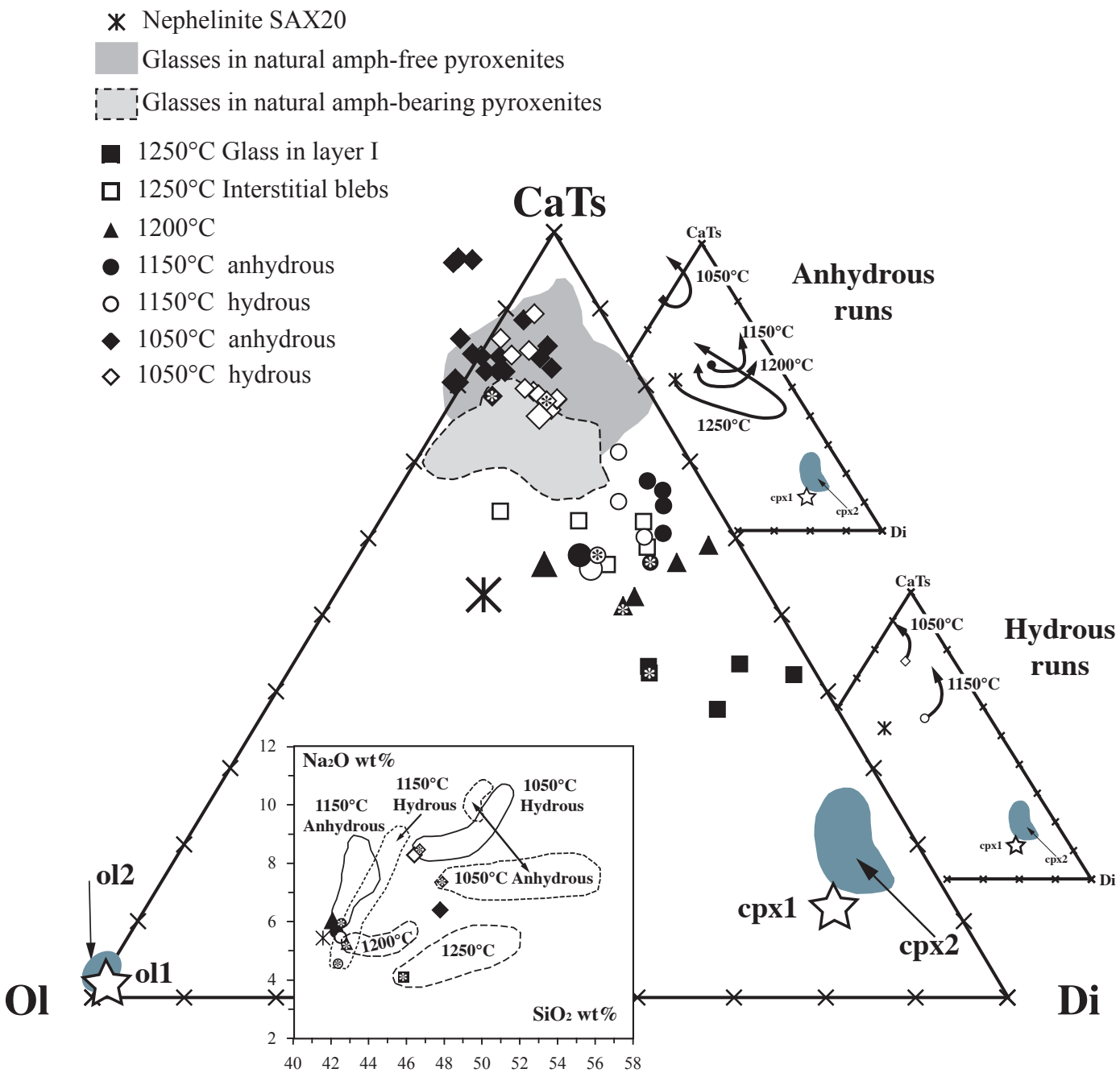

Fig. 7
Perinelli et al.

Table 1. *Representative composition of minerals in lherzolite and in wehrlite together with whole rock composition of nephelinite SAX20 and other synthetic starting materials used in the runs. Metasomatising melts inferred by Coltorti et al., (2004) are also reported for comparison.*

	Lherzolite 154L				***Wehrlite BRP19***			***SAX20***	***SAX20glass_5bru***	***SAX20-2.5TiO$_2$glass_5bru***	*melt1*	*melt2*
note	ol1	opx1	cpx1	sp1	ol1	cpx1	sp1	1	nominal	nominal	3	3
SiO_2	40.73	55.93	52.81	bdl	40.55	51.18	0.05	40.78	39.19	38.23	39.68	47.74
TiO_2	bdl	bdl	0.07	0.01	bdl	0.67	2.18	3.62	3.48	5.74	7.48	5.66
Al_2O_3	bdl	3.25	3.19	48.04	bdl	4.16	26.84	11.81	11.35	11.07	12.13	10.49
FeO^T	8.79	5.59	1.93	11.32	17.57	6.01	28.53	14.50	13.93	13.59	3.74	5.66
MnO	0.09	0.18	0.14	0.02	0.19	0.10	0.10	0.28	0.27	0.26		
MgO	50.20	34.17	16.99	18.49	41.53	16.43	11.42	9.33	12.26	12.04	17.91	13.32
CaO	0.02	0.55	23.56	bdl	0.18	19.75	bdl	9.23	8.87	8.65	14.96	9.9
Na_2O	n.d.	0.04	0.39	n.d.	n.d.	0.64	n.d.	5.31	5.10	4.98	4.04	4.01
K_2O	bdl	bdl	bdl	bdl	bdl	bdl	bdl	1.54	1.48	1.44		2.83
Cr_2O_3	bdl	0.66	0.79	20.76	bdl	0.92	29.99	0.08	0.08	0.08		
NiO	0.40	n.d.	n.d.	n.d.	bdl	bdl	bdl	0.03	0.03	0.03		
P_2O_5	n.d.	n.d.	n.d.	n.d.	n.d.	n.d.	n.d.	1.60	1.54	1.50		
H_2O	n.d.	n.d.	n.d.	n.d.	n.d.	n.d.	n.d.	0.90	1.47	1.47		
Tot	100.23	100.37	99.87	98.64	100.02	99.86	99.11	99.01	99.05	99.08	99.94	99.61
Fo	91.05				80.81							
En		90.38	48.44			48.26						
Fs		8.57	3.31			10.07						
Mg#				0.75			0.50					
Cr#				0.22			0.43					

Note: ol1 = olivine; opx1 = orthopyroxene; cpx1 = clinopyroxene; sp1 = spinel; 1: from Orlando et al., (1997). H_2O value refers to LOI. 2 = average and standard deviation (st. dev.) of 3 analyses of the glass produced from Ti doped SAX20; 3 = metasomatising melts from Coltorti et al., (2004). bdl = below detection limit; n.d.= not determined, Fo, En, Fs represent forsteritic, enstatitic, ferrosilitic components, respectively. Mg#= Mg/(Mg+Fe), Cr#= Cr/(Cr+Al).

Table 2. *Experimental assemblage, run conditions and results.*

Run	*Starting Material*	*Capsule*	*P(GPa)*	*T(°C)*	*Dur.(h)*	*Detected phases*
169	154L SAX20	C-Pt	1.5	1150	3	lh: ol1, opx1, cpx1, sp1, cpx2, sp2 nf: glass, cpx, ol, sp, ne
167	154L SAX20	C-Pt	1.5	1200	4	lh: ol1, opx1, cpx1, sp1, cpx2, sp2 nf: glass, cpx, ol, sp
170	154L SAX20	C-Pt	1.5	1250	49	lh: ol1, opx1, cpx1, sp1, cpx2, sp2, <<glass nf: glass, cpx, ol
166	154L SAX20	C-Pt	1.5	1300	75	lh: ol1, opx1, cpx1, sp1, cpx2, sp2, <<glass nf: glass
173	154L SAX20	C-Pt	2.0	1300	95	lh: ol1, opx1, cpx1, sp1, cpx2, sp2 nf: glass, cpx, ol, rhönite, sp
178	*154L* *SAX20-2.5TiO2glass_5bru*	$Ag_{50}Pd_{50}$	2.0	975	212	lh: ol1, opx1, cpx1, sp1, cpx2, sp2 nf: glass, ol, cpx, sp
177	*154L* *SAX20-2.5TiO2glass_5bru*	$Ag_{50}Pd_{50}$	2.0	1025	190	lh: ol1, opx1, cpx1, sp1, (ol2), (opx2), cpx2, sp2, <glass2 nf: glass, oxides, cpx, ap
176	*154L* *SAX20glass_5bru*	$Ag_{50}Pd_{50}$	2.0	1025	190	lh: ol1, opx1, cpx1, sp1, (ol2), (opx2), cpx2, sp2, <glass2 nf: glass, ol, cpx, rhönite, ap
141	BRP19 SAX20	C-Pt	1.0	1250	5	py: ol1, cpx1, ol2, cpx2, glass nf: glass
140	BRP19 SAX20	C-Pt	1.0	1200	8	py: ol1, cpx1, ol2, cpx2, <glass nf: glass, ol
144	BRP19 SAX20	C-Pt	1.0	1175	8	py: ol1, cpx1, ol2, cpx2, <glass nf: glass, ol
150	BRP19 SAX20	C-Pt	1.0	1150	8	py: ol1, cpx1, ol2, cpx2, <glass nf: glass, ol, cpx, oxides
153	BRP19 SAX20	C-Pt	1.0	1150	24	py: ol1, cpx1, ol2, cpx2, glass nf: glass, ol, cpx, oxides
154	BRP19 SAX20	C-Pt	1.0	1050	48	py: ol1, cpx1, ol2, cpx2, glass nf: glass, ol, cpx, oxides, ne
153*	BRP19 SAX20	C-Pt	1.0	1150	24	py: ol1, cpx1, ol2, cpx2, glass nf: glass, ol, cpx, oxides
154*	BRP19 SAX20	C-Pt	1.0	1050	48	py: ol1, cpx1, ol2, cpx2, glass, < sp2 nf: glass, ol, cpx, oxides, rhönite, ap

C-Pt: double capsules with graphite inside Pt, Dur.=duration, *lh*, *nf*, *py* in the *Detected phases* column refer to phases found in lherzolitc (lh), nephelinitic (nf) and pyroxenitic (py) portions of the capsule. ol= olivine, opx= orthopyroxene, cpx= clinopyroxene, sp= spinel, ap= apatite, ne= nepheline. The suffixes *1* and *2* refer to original and neo-formed phases, respectively. "<" = scarce; "<<" = rare; * = experiments with ~ 3 wt% H_2O added in the charge.

Table 3. *Representative electron microprobe analyses of cpx2 (a), sp1 and sp2 (b) and glasses (c) in lherzolite.*

a) Run	169	169	169	167	167	167	167	167	170	170	166	
P(GPa)/T(°C)	1.5/1150	1.5/1150	1.5/1150	1.5/1200	1.5/1200	1.5/1200	1.5/1200	1.5/1200	1.5/1250	1.5/1250	1.5/1300	
SiO_2	54.59	54.29	53.51	47.67	53.39	53.97	54.10	54.19	54.31	54.34	53.27	
TiO_2	bdl	bdl	0.11	2.35	0.17	0.18	0.41	0.03	0.18	0.20	0.09	
Al_2O_3	0.71	0.70	1.94	8.82	3.98	4.06	4.49	2.96	3.24	4.92	3.23	
Cr_2O_3	1.91	1.47	0.83	0.81	1.93	1.82	0.86	1.85	1.20	2.71	1.77	
FeO^T	2.44	2.58	3.18	7.39	5.59	5.54	6.21	5.73	4.28	3.24	3.57	
MnO	0.32	0.14	bdl	0.22	0.08	0.17	0.28	0.30	0.28	0.23	0.11	
MgO	19.42	19.19	19.29	14.02	22.63	21.96	22.00	25.96	20.42	17.00	20.11	
CaO	19.91	20.79	20.13	15.96	10.51	11.17	10.71	7.62	14.77	15.37	16.95	
Na_2O	0.70	0.83	0.59	2.31	1.17	1.23	1.47	0.83	1.04	2.24	0.93	
K_2O	0.04	bdl	0.04	0.14	bdl	bdl	0.09	bdl	bdl	bdl	bdl	
Tot	100.04	99.99	99.62	99.69	99.45	100.10	100.62	99.47	99.72	100.25	100.03	
mg#	93.39	92.96	91.50	77.10	87.78	87.55	86.27	88.94	89.43	90.30	90.90	
SiO_2/Al_2O_3	76.89	77.56	27.58	5.40	13.41	13.29	12.05	18.31	16.76	11.04	16.49	
Run	178	178	176	176	176	177	177	173	173	173	173	173
P(GPa)/T(°C)	2/975	2/975	2/1025	2/1025	2/1025	2/1025	2/1025	2/1300	2/1300	2/1300	2/1300	2/1300
SiO_2	54.06	54.49	54.95	54.95	53.40	54.83	53.53	51.66	53.18	53.65	53.77	53.43
TiO_2	0.05	0.08	0.09	0.11	0.17	0.29	0.87	1.38	0.37	0.57	0.66	0.10
Al_2O_3	3.28	2.91	1.65	1.60	4.20	3.85	6.18	7.88	7.13	7.30	8.39	6.44
Cr_2O_3	0.75	1.05	2.52	2.31	0.64	0.97	2.08	1.09	1.66	1.29	1.29	1.83
FeO^T	1.86	1.94	2.20	2.24	3.70	3.79	5.75	8.84	4.20	4.25	4.13	3.78
MnO	0.05	0.06	0.09	0.21	0.26	0.14	0.17	0.29	0.17	0.21	0.15	0.06
MgO	17.41	16.93	18.25	18.83	16.55	16.46	14.08	14.72	18.36	17.55	17.37	18.05
CaO	20.72	21.46	19.43	18.96	18.60	18.13	14.02	11.12	11.97	10.93	9.72	14.18
Na_2O	1.53	1.34	1.25	1.27	1.89	2.45	3.90	3.41	2.75	3.63	4.14	2.27
K_2O	0.19	0.27	bdl	bdl	0.04	bdl	bdl	0.07	bdl	bdl	bdl	0.04
Tot	99.90	100.53	100.43	100.48	99.45	100.91	100.58	100.46	99.79	99.38	99.62	100.18
mg#	94.32	93.93	93.64	93.72	88.81	88.51	81.29	74.71	88.58	87.99	88.18	89.44
SiO_2/Al_2O_3	16.48	18.73	33.30	34.34	12.71	14.24	8.66	6.56	7.46	7.35	6.41	8.30

Note: mg#= $Mg*100/(Mg+Fe^T)$, bdl= below detection limit.

Table 3. *continued*

b) Run	169	169	167	170	173	176	176	176	177	177	178
Phase	sp1	sp2	sp2	sp1	sp1	sp1	sp2	sp2	sp2	sp2	sp1
P(GPa)/T(°C)	1.5/1150	1.5/1150	1.5/1200	1.5/1250	2/1300	2/1025	2/1025	2/1025	2/1025	2/1025	2/975
TiO_2	0.07	0.11	0.11	0.59	0.32	0.10	0.15	0.07	1.81	1.21	bdl
Al_2O_3	46.42	35.42	22.56	44.05	42.63	46.83	33.68	24.29	14.68	15.89	49.45
Cr_2O_3	22.89	36.15	47.64	22.40	27.73	22.84	32.62	42.74	41.53	41.40	21.67
FeO^T	12.43	12.77	11.79	17.25	11.54	12.06	20.49	18.60	31.57	31.04	10.78
MnO	0.11	0.15	0.16	0.14	0.08	0.13	0.42	0.32	0.47	0.51	0.13
MgO	18.68	17.30	16.67	15.18	18.49	18.93	13.72	13.14	10.49	10.84	19.81
CaO	0.02	0.06	0.14	0.15	0.02	0.07	0.14	0.05	0.12	0.08	0.00
Tot	100.62	101.96	99.07	99.76	100.79	100.96	101.22	99.21	100.67	100.97	101.84
Cr#	0.25	0.41	0.59	0.25	0.30	0.25	0.39	0.54	0.65	0.64	0.23
Mg#	0.75	0.72	0.75	0.63	0.75	0.76	0.59	0.60	0.48	0.50	0.78

Note: Mg#= $Mg/(Mg+Fe^{2+})$ where Fe^{2+} was calculated on the basis of stoichiometry and charge balance,
Cr#= Cr/(Cr+Al), bdl= below detection limit.

Table 3. *continued*

c) Run	170	170	170
P(GPa)/T(°C)	1.5/1250	1.5/1250	1.5/1250
SiO_2	54.64	56.96	58.27
TiO_2	1.37	0.55	0.44
Al_2O_3	21.55	21.47	22.26
Cr_2O_3	bdl	0.08	0.13
FeO	3.61	2.90	2.58
MnO	0.11	bdl	0.03
MgO	3.58	3.10	3.49
CaO	2.72	2.04	2.05
Na_2O	4.38	4.99	5.31
K_2O	3.68	3.91	4.29
Tot	95.64	96.00	98.85

Note: bdl= below detection limit.

Table 4. *Representative electron microprobe analyses of ol2 (a), cpx2 (b) and glasses (c) in wehrlite.*

a) Run	141 ol[a]	141 ol[b]	141 ol2	141 ol[c]	140 ol2[d]	140 ol2	140 ol2[d]	153 ol2[d]	153 ol2[e]	153 ol2[d]	153* ol2[d]	153* ol2
T(°C)	1250	1250	1250	1250	1200	1200	1200	1150	1150	1150	1150	1150
SiO_2	39.06	39.57	40.19	40.02	38.77	38.56	38.69	37.99	38.53	39.21	38.19	38.88
TiO_2	bdl	bdl	bdl	bdl	0.02	0.14	0.03	bdl	bdl	bdl	bdl	bdl
Al_2O_3	0.12	bdl	bdl	bdl	0.09	0.32	0.03	0.04	0.03	0.03	0.24	0.05
FeO	16.00	14.58	15.43	14.33	23.16	23.95	21.36	22.91	21.18	19.85	21.21	24.00
MnO	0.39	0.21	0.3	0.1	0.42	0.4	0.49	0.36	0.37	0.34	0.48	0.44
MgO	42.75	44.1	44.09	44.77	36.43	35.83	38.86	37.07	39.57	39.81	38.32	36.91
CaO	0.42	0.39	0.58	0.35	0.44	0.5	0.32	0.62	0.56	0.47	0.54	0.50
NiO	0.24	0.18	0.12	0.18	0.27	0.19	0.19	0.1	0.15	0.23	bdl	0.11
Cr_2O_3	0.17		0.2	0.12	0.04	0.02	bdl	0.09	0.14	0.02	0.12	0.07
Tot	99.15	99.03	100.91	99.87	99.64	99.91	99.97	99.18	100.54	99.96	99.1	100.94
Fo	82.65	84.36	83.59	84.78	73.71	72.73	76.43	74.26	76.91	78.14	76.31	73.28
	154 ol2	154 ol2[e]	154 ol2[e]	154* ol2	154* ol2	154* ol2[e]	154* ol2[e]					
T(°C)	1050	1050	1050	1050	1050	1050	1050					
SiO_2	37.25	37.57	39.81	37.69	38.16	39.83	39.63					
TiO_2	bdl	bdl	bdl	bdl	bdl	bdl	bdl					
Al_2O_3	0.03	0.22	0.02	0.02	0.19	bdl	0.25					
FeO	32.52	28.82	20.16	30.69	27.68	19.30	17.84					
MnO	0.73	0.59	0.35	0.56	0.43	0.34	0.21					
MgO	28.99	32.31	39.35	30.59	33.46	40.10	41.18					
CaO	0.53	0.43	0.23	0.50	0.41	0.35	0.07					
NiO	0.02	0.09	0.17	0.09	0.1	0.19	0.17					
Cr_2O_3	0.1	bdl	0.2	bdl	0.08	bdl	0.22					
Tot	100.18	100.03	100.29	100.14	100.51	100.10	99.57					
Fo	61.38	66.64	77.67	63.99	68.31	78.81	76.43					

Note; * = wet experiments; Fo= forsterite; bdl= below detection limit. a) restitic olivine in layer I; b) restitic olivine in layer II; c) restitic olivine in layer III; d) analysis at the rim of ol1 at nephelinite/wehrlite boundary layer; e) away to nephelinite/wehrlite boundary layer

Table 4. *Continued*

b) Run	141	141	141	140	140	153	153	153*	153*	154	154	154
	cpx restitic	cpx2[a]	cpx2[a]	cpx2[b]	cpx2[c]	cpx2[c]	cpx2[a]	cpx2[c]	cpx2[b]	cpx2[c]	cpx2[c]	cpx2[a]
T(°C)	1250	1250	1250	1200	1200	1150	1150	1150	1150	1050	1050	1050
SiO_2	54.11	47.89	50.09	50.54	49.63	46.73	50.88	48.57	51.56	45.29	47.76	50.63
TiO_2	0.28	2.71	1.45	1.25	1.08	2.84	1.55	2.47	1.24	3.92	2.30	1.12
Al_2O_3	1.46	6.17	4.79	5.44	4.91	7.72	5.03	5.54	3.38	7.90	6.61	4.87
Cr_2O_3	1.39	0.31	0.23	0.88	0.88	0.57	0.73	0.28	0.75	0.07	0.15	0.65
FeO^T	4.17	10.24	8.75	6.55	6.24	6.13	4.93	7.79	5.73	9.13	8.24	6.42
MnO	0.10	0.36	0.23	0.16	0.11	bdl	0.07	0.11	0.05	0.26	0.33	bdl
MgO	16.35	11.24	13.52	14.44	15.84	12.80	14.51	12.75	15.19	10.31	12.73	15.22
CaO	21.05	20.14	19.51	19.93	20.44	21.71	21.37	20.83	21.81	22.41	20.46	19.71
Na_2O	0.55	1.40	1.54	0.74	0.81	1.19	1.11	1.18	0.64	1.00	1.15	0.83
Tot	99.46	100.46	100.11	99.93	99.95	99.69	100.18	99.53	100.36	100.29	99.73	99.45
mg#	87.49	66.18	73.37	79.72	81.90	78.83	83.99	74.48	82.54	66.81	73.36	80.87
SiO_2/Al_2O_3	37.06	7.76	10.46	9.29	10.11	6.05	10.12	8.77	15.25	5.73	7.23	10.40

	154*	154*	154*	154*
	cpx2[c]	cpx2[c rim]	cpx2[c]	cpx2[b]
T(°C)	1050	1050	1050	1050
SiO_2	46.94	45.83	44.53	46.91
TiO_2	2.70	2.49	5.33	2.94
Al_2O_3	7.54	8.95	10.64	7.80
Cr_2O_3	bdl	bdl	0.42	0.08
FeO^T	9.65	8.78	7.70	9.30
MnO	0.19	0.13	0.16	0.25
MgO	10.30	10.61	9.60	10.30
CaO	21.52	21.43	20.99	20.79
Na_2O	1.04	1.11	1.29	1.32
Tot	99.88	99.33	100.66	99.67
mg#	87.49	66.18	73.37	79.72
SiO_2/Al_2O_3	37.06	7.76	10.46	9.29

Note: mg#= Mg*100/(Mg+FeT) bdl= below detection limit; a) cpx2 neocrysts in glass blebs far from SAX20/wehrlite boundary layer; b) clinopyroxene reacted rim analysed far from SAX20/wehrlite boundary layer; c) cpx2 at boundary layer.

Table 4. *Continued*

c) Run	141 glass[a]	141 glass[a]	141 glass[a]	141 glass[b]	141 glass[b]	141 glass[b]	141 glass[b]	140 nephelinite derived melt	140 glass[a]	140 glass[b]	153 nephelinite derived melt	153 glass[a]	153 glass[b]
T(°C)	1250	1250	1250	1250	1250	1250	1250	1200	1200	1200	1150	1150	1150
SiO_2	45.86	46.28	48.26	47.34	49.23	50.63	51.69	42.24	45.12	46.28	42.4	42.56	44.52
TiO_2	2.66	2.47	2.05	2.72	2.15	1.95	2.13	3.48	4.09	3.91	4.23	4.25	4.36
Al_2O_3	9.74	9.34	8.29	9.84	9.12	13.13	13.34	13.21	13.88	14.16	14.07	13.94	14.67
Cr_2O_3	0.22	0.76	0.28	0.26	0.35	0.52	0.06	0.06	0.1	bdl		0.05	bdl
FeO^T	13.64	13.47	13.14	12.37	12.13	17.28	13.38	14.35	11.84	11.84	13.85	12.74	11.41
MnO	0.23	0.29	0.26	0.23	0.31	0.35	0.25	0.34	0.31	0.25	0.25	0.28	0.37
MgO	9.11	9.42	8.13	6	5.10	2.01	1.2	6.58	4.82	3.15	4.56	3.63	1.74
CaO	12.24	12.45	13.64	14.52	14.49	7.61	9.47	10.22	12.82	12.81	11.73	12.66	11.45
Na_2O	4.1	4.17	4.37	4.78	5.56	4.62	5.34	5.90	5.19	5.6	5.69	5.94	7.32
K_2O	1.17	1.16	1.06	1.12	1.25	1.84	2.37	1.96	1.84	1.99	1.95	2.35	2.48
P_2O^5	1.03	0.19	0.5	0.83	0.30	0.06	0.78	1.64	na	na	1.28	1.61	1.68
mg#	54.35	55.49	52.45	46.37	42.83	17.16	13.79	44.98	42.06	32.17	36.99	33.69	21.38
SiO_2/Al_2O_3	4.71	4.96	5.82	4.81	5.40	3.86	3.87	3.20	3.25	3.27	3.01	3.05	3.03
	153* nephelinite derived melt	153* glass[a]	153* glass[b]	154 nephelinite derived melt	154 glass[a]	154 glass[a]	154 glass[b]	154 glass[c]	154* nephelinite derived melt	154* glass[a]	154* glass[a]	154* glass[a]	154* glass[b]
T(°C)	1150	1150	1150	1050	1050	1050	1050	1050	1050	1050	1050	1050	1050
SiO_2	42.60	43.93	45.76	47.85	49.76	49.4	55.03	50.2	46.74	47.59	48.26	49.9	51.25
TiO_2	3.85	3.94	3.31	2.40	1.88	2.45	1.46	1.69	2.56	2.46	2.20	2.11	1.73
Al_2O_3	13.14	15.28	16.69	19.40	21.01	20.15	22.31	21.75	19.43	19.76	19.98	21.51	23.13
Cr_2O_3	0.14	0.01	bdl	0.03	bdl	0.16	0.04	bdl	bdl	0.08	bdl	0.11	0.07
FeO^T	13.97	10.92	9.49	11.20	6.67	9.33	3.4	5.76	10.26	9.57	9.04	6.76	4.44
MnO	0.30	0.17	0.25	0.18	0.06	0.2	0.01	0.03	0.23	0.26	0.23	0.21	0.09
MgO	5.85	3.26	1.77	2.20	1.96	1.86	1.66	1.95	2.22	2.23	2.30	2.02	1.7
CaO	11.49	11.79	9.62	6.07	4.53	5.36	2.79	3.68	6.58	5.89	5.75	4.93	3.58
Na_2O	5.43	6.61	8.81	6.47	9.62	6.97	7.92	10.51	8.45	8.54	8.37	8.79	10.31
K_2O	2.00	2.04	2.05	3.10	3.67	3.44	4.45	3.82	2.94	3.07	3.12	3.66	3.7
P_2O^5	1.24	2.06	2.26	1.11	0.84	0.68	0.92	0.6	0.60	0.54	0.76	0.45	0.37
mg#	42.75	34.74	24.95	25.97	34.36	26.22	46.54	37.64	27.84	29.35	31.22	34.76	40.57
SiO_2/Al_2O_3	3.24	2.88	2.74	2.47	2.37	2.45	2.47	2.31	2.41	2.41	2.42	2.32	2.22

Note: mg#= Mg*100/(Mg+FeT); bdl= below detection limit. na= not analysed a) glass blebs at SAX20/wehrlite boundary layer; b) glass blebs in the wehrlite layer; c) glass analysed along the capsule wall (see the text).